C.P. No. 1024

MINISTRY OF TECHNOLOGY

AERONAUTICAL RESEARCH COUNCIL

CURRENT PAPERS

An Investigation of Stress Redistribution Caused by Creep in a Thick-Walled Circular Cylinder Subjected to Axial and Thermal Loading

By

J. M. Clarke

An investigation of stress redistribution caused by creep
in a thick-walled circular cylinder subjected
to axial and thermal loading

- by -

J. M. Clarke

SUMMARY

A thick-walled tube was subjected to an axial load and a radial
temperature distribution which caused thermal stresses. The creep
strains and the eventual rupture times were observed and compared with
conventional creep tests and theoretical analysis. Theory suggested and
experiments confirmed that stress redistribution caused the overall strain
behaviour to approach that for the mean axial stress and the mean radial
temperature.

Description of the experimental technique and apparatus includes a
novel and simple optical extensometer. Appendices contain a complete
analytic treatment of the triaxial stress problem in a long thick tube in
the presence of an arbitrary distribution of non-elastic strains, and a
treatment of some conditions under which stress-redistribution calcula-
tions can lead to a "steady state" or "fully redistributed" stress pattern.

A less rigorous theoretical treatment which ignores radial con-
straints is shown to lead to an under-estimate of the thermal stresses and
of the time required for stress redistribution to occur.

CONTENTS

Detachable Abstract Cards

TABLES

APPENDICES

ILLUSTRATIONS

ILLUSTRATIONS (cont'd)

1.0   Introduction

The application of the digital computer to stress analysis allows
solutions to be obtained easily to a large number of problems which have
to be tackled by numerical methods. One example is the redistribution of
stress in an internally cooled gas turbine rotor blade[1]. This redistri-
bution is caused by the accumulation of creep strains at different rates
which depend on the temperature, stress and previous history of each
element of the blade. The most important result of the stress redistri-
bution process is that the stress pattern becomes more uniform than that
calculated simply on a basis of the thermal strains and a perfectly
elastic material. This is illustrated for a very simple tensile system
on Figure 1. By consideration of rupture times based on the most severe
conditions of stress and temperature within a blade the stress pattern can
be shown to become more favourable as redistribution proceeds; furthermore
the redistribution is predicted to be complete before any part of the blade
would be expected to fail. The time to rupture of the blade should there-
fore be more closely related to the mean stress and mean temperature at a
spanwise position than to the most severe combination of stress and tem-
perature at the beginning of redistribution.

In order to obtain some guidance to the validity of the assumptions
and to compare the predicted rupture life with that actually observed, an
experimental and theoretical investigation has been conducted on a thick-
walled circular cylinder subjected to an axial tensile load and a radial
temperature gradient. Apart from being worthy of study in its own right,
the choice of a cylindrical geometry made the problem amenable to analysis
while corresponding closely to the geometrically more complex situation
within a cooled turbine rotor blade. It also enabled an experiment to be
conducted under carefully controlled laboratory conditions and strain
measurements to be taken. Confirmation that the accumulation of axial
creep strain and the observed rupture lives agree well with those based on
the conditions of mean stress and temperature are the most important
results from this experimental investigation.

Figure 2 shows a schematic arrangement of the apparatus used. The
axial load was applied by a 5-ton Denison creep machine and the radial
temperature gradient was produced by passing an electrical current axially
along the test specimen and allowing the latter to radiate freely from its
outside surface. A number of experiments were repeated to determine scat-
ter and some control experiments were made to separate variables, the whole
programme involving about 5000 hr of creep testing.

2.0   Experimental

2.1   Design of the experiment

The dimensions, temperatures and stresses used for the experiment
were chosen to satisfy,

(i)   a modest electric power requirement

(ii)   tight manufacturing tolerances, especially in the bore of
       the test specimen

(iii) mean stress and temperature sufficient to cause rupture in
       about 400 hr if redistribution occurred

(iv)   a combination of local stress and temperature severe enough
       to initiate rupture in a much shorter time if redistribution
       did not occur

(v)   the temperature to be high enough to cause the required
       radiation intensity from the outside surface.

A number of exploratory calculations using manufacturer's data for
Nimonic alloy 105 led to the choice of the following values:-

tube length	3 in.
inside diameter	$\frac{n}{16}$ in.
outside diameter	$\frac{5}{8}$ in.
mean axial stress	4 ton/in^2
maximum axial stress	7 ton/in^2
mean temperature	950°C

For these conditions the rupture times for the most severe (initial)
stress and temperature and the mean stress and temperature were estimated
to be 40 hr and 400 hr respectively. The calculations showed that there
was very little freedom to depart from the chosen values.

The tests on tubular specimens containing a radial temperature
gradient (Type 1 tests) were supported by four other test arrangements
intended to act as controls and to provide creep data for the same batch
of material. They are shown on Figure 3.

Type 2 tests simulated Type 1 except for the provision of external
insulation and an auxiliary heater to ensure a uniform radial temperature.
These tests were therefore free from thermal stresses.

The single Type 3 test also used a tubular specimen but heated it
in a conventional creep test furnace.

Type 4 and 5 tests used solid cylindrical specimens of two different
types to establish the creep strain behaviour of the material. The test
technique conformed with orthodox creep test methods.

2.2 Control and measurement of temperature

The temperature sensitivity of rupture times, at the chosen mean stress and temperature levels, was 4·5 per cent reduction in life per $^{\circ}$C rise in temperature. The temperature of the furnace heated specimens was generally controlled within $\pm\frac{1}{2}^{\circ}$C and that of the tube tests within approximately $\pm 1^{\circ}$C. Platinum resistance thermometers were used as sensors for the proportional temperature controllers but temperature measurements were made using platinum/platinum rhodium thermocouples. For the radiating tube tests three such thermocouples were lightly welded to the bore, and for the others the thermocouples were tied to the specimen surface and shielded against direct radiation from the furnace walls. The temperature difference between inside and outside surfaces of the tube was calculated using the measured electrical power and the manufacturer's data for thermal conductivity.

2.3 Development of the apparatus

The calculation of temperature difference referred to in the last section assumed no loss of heat from the gauge length (the central $\frac{5}{8}$ in.) by conduction along the tube axis. It was therefore necessary to ensure a uniform temperature for about an inch in the centre of the tube length. This was achieved, after some abortive attempts with auxiliary end heaters, by providing insulating collars at the ends as shown in Figure 4. These collars reduced radiant heat loss in the areas where conduction was causing lower temperatures. Figure 5 shows the longitudinal temperature profiles obtained under various conditions. Preliminary creep tests showed the material to be considerably stronger than the manufacturer's data implied and for this reason the test temperatures were raised by 20°C to return the rupture times to the values originally intended.

2.4 Measurement of strain

It was felt desirable to measure strains on the radiating specimens if this could be done without interfering with the symmetry of heat flux. For this purpose a simple and novel optical extensometer was constructed (see Figure 6).

The principle employed was the displacement of a light path by the interposition of inclined glass blocks as shown on Figure 7. One pair of fixed blocks served to superimpose the images while a second pair of thinner blocks was rotated to accommodate and measure strains. When used to observe an object illuminated by white light it was necessary to insert a dark red filter to reduce diffraction effects but when observing a red-hot specimen this was not so critical.

During the experiment both diametral and longitudinal strains were measured by simply rotating the instrument about its optical axis. The gauge length for diametral strain was defined clearly by the edges of the tube, and two circumferential platinum wires were lightly welded to the outside of the tube $\frac{5}{8}$ in. apart to define the axial gauge length. It was found that resolution was limited by clarity of the objects observed and could have been improved by using small bright sources of additional illumination (preferably monochromatic).

Because the position of coincidence of the two images in the tele-
scope eye-piece required judgement several readings (usually three) were
taken on each occasion. Best fitting curves of strain versus time were
obtained by using the fourth order polynomial with the least sum of the
squares of the errors. Subsequently histograms were constructed of the
errors relative to these curves and it was found that the 50 per cent
certainty band had width about ±0·025 per cent for the diametral strains
and ±0·050 per cent for the axial strains. The former was more accurate
because the gauge length was more clearly defined. These values are
maximum values because they include not only instrument errors but also
errors due to the fitted curve being too smooth and therefore possibly
masking real effects.

In order to measure the strains during the Type 4 tests, use was
made of transducers attached to a design of extensometer described in
Reference 3 and widely used at N.G.T.E.

2.5 Results

The results for individual tests are distinguished by code letters.
The key to these letters is given on Figure 21 which folds out for use
with Figures 8, 9, 12 and 13. Comments on the results are postponed
until Section 4.0.

2.5.1 Rupture times and reductions of area

The rupture times and reductions of area are given in Table I
together with the test conditions. The same rupture time information is
shown graphically on Figures 8 and 9 with the temperatures measured by
the thermocouple nearest to the eventual rupture line.

2.5.2 Strain records

Only two strain records were obtained from the three Type 1 tests
because the first was completed before the construction of the optical
extensometer. Figures 10 and 11 show the results. For the small
strains the scale has been magnified. The short vertical lines on the
figures show the range between the greatest and least strains measured on
each occasion.

Type 2 tests were enclosed by lagging so that strain measurement
using the optical extensometer was not possible.

Figures 12 and 13 show the creep strain readings for the Type 4
and 5 tests at the two different conditions of stress and temperature.

2.5.3 Micrographs

Micrographic sections were taken off several specimens and three
of these are shown in Figures 14 and 15. Figure 14 from specimen C
illustrates the typical creep type rupture caused by cracking at the
grain boundaries. There are no obvious peculiarities attributable to
the electrical heating technique.

Figure 15 confirms a difference between the inside and outside con-
ditions in Test C. It shows more extensive oxidation on the inside sur-
face; indeed this surface of C was more severely attacked than any other.

3.0 Theoretical

3.1 Some order of magnitude considerations

Using manufacturer's data for Nimonic alloy 105 at 970°C it may be
shown that a strain of 0·06 per cent may be caused by:-

either	elastic strain from a uniaxial stress of 5 ton/in^2
or	creep strain after about 5 hr at 5 ton/in^2
or	a temperature difference of 15°C.

The equal strains caused by the conditions listed above, all of
which are fairly easily realised, show that the behaviour of a hot compo-
nent is typified by a strong interaction between elastic, thermal expan-
sion and creep effects. At lower temperatures it would also be necessary
to consider plastic flow.

3.2 Stress analysis

The elastic thermal stress analysis of a long thick cylinder is
available from standard texts[4] for an arbitrary radial temperature distri-
bution. The temperature influences the stress pattern by introducing
thermal strains. Whereas thermal strains are concerned with volume
changes, creep strains are concerned with shape changes and it was there-
fore necessary to extend the solution. Appendix II gives details of the
extended analysis. The approach is analytical rather than numerical but
completely closed forms of solution for the stresses are obtainable only
if analytic functions are assumed for the distributions of the various non-
elastic strains. In practice these distributions were represented by
arrays of numbers within a digital computer and the accuracy of solution
then depends on the extent of these arrays and the numerical method used
for their integration.

The stress analysis does not need to distinguish the various (e.g.,
thermal, plastic, creep) components of non-elastic strain and the procedure
adopted in the theoretical work described here was to add together the
terms caused by thermal expansion and creep at any instant prior to the
calculation of the corresponding stress pattern. Implicit assumptions in
the analysis are that the non-elastic strains should be small enough to
permit the usual tensor representation and that the principal directions of
non-elastic strain must coincide with those of the elastic stresses and
strains, namely the hoop radial and axial directions. Furthermore, the
material is assumed to be elastically and plastically isotropic.

3.3 Calculation of creep strain increments

Creep behaviour is still described in empirical terms and compre-
hensive results from creep tests of materials such as nickel base alloys
are only available for tests at constant stress and temperature under uni-
axial tensile conditions. In stress redistribution studies, involving a

changing pattern of multiaxial stresses, it is necessary therefore to augment the data by using certain hypotheses in order to

(a)   permit estimates of behaviour under changing uniaxial conditions and

(b)   permit predictions of behaviour under multiaxial stress situations including compression.

The hypotheses used in the work described here are not new and are reproduced here simply for completeness.

3.3.1 Time and strain hardening hypotheses

These are two of the many alternative hypotheses currently being considered. For more complete descriptions of them see for instance References 5, 6, 7, 8 and 9.

Suppose creep strain data from tests at constant stress and temperature are available in the form

$$\varepsilon = f(\sigma, T, t) \qquad \qquad ....(1)$$

where ε is creep strain

σ is stress (uniaxial tensile)

T   is temperature

t   is time measured from application of the load

f   is a function with σ, T and t as variables

then in principle the same information can also be expressed as

$$t = g(\sigma, T, \varepsilon) \qquad \qquad ....(2)$$

where   g   is a different function.

According to the "time hardening" hypothesis the increment of creep strain caused by a period (Δt) of constant stress (σ_1) and temperature (T_1) following the instant at which the strain was ε_1 and the time was t_1 is given by

$$\Delta \varepsilon_t = f(\sigma_1, T_1, t_1 + \Delta t) - f(\sigma_1, T_1, t_1)$$

$$= f_t(\sigma_1, T_1, t_1, \Delta t) \qquad \qquad ....(3)$$

where the subscript t refers to time hardening.

According to the "strain hardening" hypothesis the increment of creep strain caused by the same conditions would be

$$\Delta \varepsilon_s = f\left(\sigma_1, \; T_1, \; g(\sigma_1, \; T_1, \; \varepsilon_1) + \Delta t\right) - \varepsilon_1$$

$$= f_s(\sigma_1, \; T_1, \; \varepsilon_1, \; \Delta t) \qquad \qquad \cdots (4)$$

where the subscript s refers to strain hardening.

It is apparent that the influence of previous loading and straining is being introduced by the single values of time (t_1) and strain (ε_1) respectively, and a convenient (non-iterative) use of the strain hardening hypothesis depends on the existence of both "f" and "g" functions. Suitable expressions are given in Reference 10. It should be noted that many forms of "f", for example sums of terms containing powers of t, do not lend themselves to conversion to "g" functions.

3.3.2 Effective stress and strain

The expressions (3) and (4) above which refer to uniaxial tensile data can be extended to multiaxial situations by postulating effective stresses $(\bar{\sigma})$ and strains $(\bar{\varepsilon})$ so that

$$\Delta \bar{\varepsilon}_t = f_t(\bar{\sigma}_1, \; T_1, \; t_1, \; \Delta t) \qquad \qquad \cdots (5)$$

$$\Delta \bar{\varepsilon}_s = f_s(\bar{\sigma}_1, \; T_1, \; \bar{\varepsilon}_1, \; \Delta t) \qquad \qquad \cdots (6)$$

where $\bar{\varepsilon}$, $\Delta\bar{\varepsilon}$ and $\bar{\sigma}$ are expressed in terms of the principal strains $(\varepsilon_1, \; \varepsilon_2, \; \varepsilon_3)$ and principal stresses $(\sigma_1, \; \sigma_2, \; \sigma_3)$ by

$$\bar{\varepsilon} = \frac{\sqrt{2}}{3} \sqrt{\left((\varepsilon_1 - \varepsilon_2)^2 + (\varepsilon_2 - \varepsilon_3)^2 + (\varepsilon_3 - \varepsilon_1)^2\right)} \qquad \cdots (7)$$

$$\Delta \bar{\varepsilon} = \frac{\sqrt{2}}{3} \sqrt{\left((\Delta\varepsilon_1 - \Delta\varepsilon_2)^2 + (\Delta\varepsilon_2 - \Delta\varepsilon_3)^2 + (\Delta\varepsilon_3 - \Delta\varepsilon_1)^2\right)}$$

$$\cdots (8)$$

and
$$\bar{\sigma} = \frac{1}{\sqrt{2}} \sqrt{\left((\sigma_1 - \sigma_2)^2 + (\sigma_2 - \sigma_3)^2 + (\sigma_3 - \sigma_1)^2\right)} \qquad \dots(9)$$

The multiplying constants being chosen so that for plastic flow under uniaxial stress,

$$\bar{\sigma} = \sigma_1 \qquad \text{when} \quad \sigma_2 = \sigma_3 = 0$$

and
$$\bar{\varepsilon} = \varepsilon_1 \qquad \text{when} \quad \varepsilon_2 = \varepsilon_3 = -\tfrac{1}{2}\varepsilon_1.$$

3.3.3 Levy-Mises flow rule

This concerns the direction of shape change and in its incremental flow form[11],[12] it ensures that the increment of effective shear strain corresponds in its direction with the current direction of effective shear stress. It may be stated in the following form,

$$\frac{\sigma_1 - \sigma_2}{\Delta\varepsilon_1 - \Delta\varepsilon_2} = \frac{\sigma_2 - \sigma_3}{\Delta\varepsilon_2 - \Delta\varepsilon_3} = \frac{\sigma_3 - \sigma_1}{\Delta\varepsilon_3 - \Delta\varepsilon_1} \qquad \dots(10)$$

It follows from the definitions of effective stress and strain that the ratio in Equation (10) also equals $2\bar{\sigma}/3\Delta\bar{\varepsilon}$.

3.3.4 Constant volume condition

Equations (5) or (6) with (7), (8), (9) and (10) suffice to determine differences between strain increments in the principal directions. In order to determine completely the actual values a further condition is required and this is taken to be the constant volume condition,

$$\Delta\varepsilon_1 + \Delta\varepsilon_2 + \Delta\varepsilon_3 = 0 \qquad \dots(11)$$

Simultaneous use of the above conditions is assured by calculating strain increments using the following expressions

$$\left. \begin{aligned}
\Delta\varepsilon_1 &= \frac{\Delta\bar{\varepsilon}}{2\bar{\sigma}} (2\sigma_1 - \sigma_2 - \sigma_3) \\[2em]
\Delta\varepsilon_2 &= \frac{\Delta\bar{\varepsilon}}{2\bar{\sigma}} (2\sigma_2 - \sigma_1 - \sigma_3) \\[2em]
\Delta\varepsilon_3 &= \frac{\Delta\bar{\varepsilon}}{2\bar{\sigma}} (2\sigma_3 - \sigma_2 - \sigma_1)
\end{aligned} \right\} \qquad \dots(12)$$

3.4   Representation of creep properties

The formulae adopted here for the description of creep properties (as measured during conventional creep strain tests at constant tensile stress and temperature) were developed in 1963 for use in the calculation of stress redistribution effects in cooled gas turbine blades, and have been found to provide an accurate and convenient method for all the Nimonic alloys[10]. They have the particular advantage which is unusual in formulae used for this purpose that while permitting a representation of both primary and tertiary creep they allow explicit evaluation of strain from time and also time from strain. The desirability of this feature was mentioned in Section 3.3.1 in connection with the use of the strain hardening hypothesis.

3.5   Evaluation of creep properties from experimental data

Because the experimental programme was concerned with a limited number of tests and a relatively small range of stresses and temperatures, it was decided to concentrate on only two different stress/temperature combinations and to do several tests at each to indicate the scatter.

Other more extensive creep strain data for Nimonic alloy 105 were available and were slightly modified in order to comply with the observed strain versus time results for this particular batch.

3.6   Computer program

A program was written in Elliott 803 Autocode to calculate, using either time or strain hardening hypotheses, the redistribution of stresses within a thick tube with non-uniform radial temperature pattern. The loading conditions on the tube are specified by

(i)   mean axial stress

(ii)   inside and outside pressures (maintained zero in this investigation)

(iii)   inside and outside radii

(iv)   temperatures at a number of equi-spaced positions through the thickness.

4.0   Discussion of experimental and theoretical results

4.1   Observed rupture times

The rupture time results fall into three categories.

(i)   Electrically heated tube specimens, both with and without radial temperature gradients and loaded by a mean axial stress of 4 t.s.i. at a mean temperature of 967·4°C broke after about 500 hr. (Tests A, B, C, D and E.)

(ii)   Furnace heated specimens with an axial stress of 4 t.s.i.
        and a temperature of 970°C broke after about 400 hr.
        (Tests F, J, K, L and N.)

(iii)   Furnace heated specimens with a stress of 7 t.s.i. and a
        temperature of 965°C broke after about 35 hr.   (Tests G,
        H, I and M.)

4.2   Observed strains

        The strain records for the two Type 1 tests shown in Figures 10
and 11 reveal a number of features:-

(i)   a very high diametral strain rate at the neck immediately
        before fracture

(ii)   necking occurred on each side of the gauge length

(iii)   examination and comparison of the diametral and axial
        strain rates suggests that there was a volumetric expansion
        in both tests for approximately the first 100 hr.   The
        magnitude of this effect was much greater for Test B than
        C but its duration was similar.   Subsequently, with the
        onset of necking (and non-uniform strain in the axial gauge
        length) the comparison between axial and diametral strains
        becomes less meaningful.   It is of interest to note that
        Levy[13] has observed an apparent volume increase in the
        early stages of creep tests on aluminium sheet material.

        The strain records for the normal creep tests are shown on
Figures 12 and 13.   The continuous lines show the hyperbolic relation
between log(strain) and log(time) which was used for the theoretical
work.

4.3   Calculated stress redistribution

        Figure 16 shows the radial temperature pattern and also the calcula-
ted stresses in the tube before, during and after stress redistribution.
Figure 17 shows the time variation of axial stress, according to both time
and strain hardening hypotheses.   The small difference between the
hypotheses as shown on Figure 18 arises from the relatively small stress
changes involved, and the fact that some stresses are increasing while
others are decreasing[14].   It has been shown elsewhere[15] that the differ-
ences are also small for turbine blade redistribution calculations,
although in that case the stress changes can be much larger.   Figure 17
also shows results calculated more simply by ignoring the radial con-
straints - that is by envisaging the tube as a set of separated concentric
tubes each with its own uniform temperature and uniaxial stress but having
the same total lengths.   It is evident that ignoring the constraints
causes an under-estimate of the thermal stresses and the time required for
redistribution.- The final distribution is unaffected because in this
example, and in the case of turbine blades, the final distribution happens
to be uniaxial.

Figure 18 shows the time variation of hoop and radial stresses and Figure 19 the directions (in the octahedral plane) of the effective stress and strain components. It is apparent that the strain direction lags behind the stress direction as a consequence of the incremental flow rule (Section 3.3.3) but they both approach the uniaxial condition.

4.4 Measured and calculated strain results

Figure 20 compares the theoretical predictions and measured values of axial strain. The upper line shows theoretical values of axial elongation according to the theory (strain and time hardening hypotheses being indistinguishable). The dashed line at the lower end depicts the results of a calculation for a cylinder without thermal stresses but having the same mean axial stress and mean radial temperature. The other continuous lines are the measured strains (transferred from Figures 10 and 11) for the tubular specimens. The lower strain level of the observed readings is associated with the direct electric heating method which seems to give consistently longer rupture times and, in part to the theoretical values used to describe the creep behaviour. Figure 12 shows the latter to give rather high creep strains in the strain range from about 1 to 10 per cent.

Examination of Figure 20 does show that application of creep data, obtained under conditions of constant stress and temperature, to a stress redistribution problem gives a strain behaviour which agrees reasonably well with that actually observed. Moreover the result of predicting the rupture life on the basis of the fully redistributed stress pattern agrees very well with the observed values. This conclusion is important because it implies that redistribution occurs as the result of very small creep strains and hence with little damage - thus confirming an assumption inherent in the present methods of calculating turbine blade lives.

5.0 Conclusions

Experimental (relevant to Nimonic alloy 105 at 970°C and 4 t.s.i.)

1. There is no significant difference between rupture times for specimens with and without modest initial thermal stresses provided that the mean stress and temperature levels are identical and do not vary with time.

2. There is a slight but consistent tendency for specimens heated directly by an electric current to last longer than those heated to the same temperature in a furnace. The life increase is equivalent to a temperature reduction of about 2°C.

3. A comparison of axial and diametral strains on the tube experiments with a temperature gradient indicates that some volume increase occurred during the first 100 hr and was particularly significant in the initial stages.

4. The shape of the strain/time curve, measured by the optical extensometer on directly heated specimens containing a radial temperature gradient, corresponded closely with that measured by conventional extensometers on furnace heated specimens containing no temperature gradient.

5.   There seemed to be no significant difference between the rupture times for the two shapes and three sizes of test specimen when all were furnace tested using the same type of testing machine.

6.   Metallurgical examination showed that the electrically heated specimens failed in a manner typical of creep at the applied stress and temperature levels.

7.   A simple optical extensometer has been made and shown capable of resolving to about ±0·025 per cent on a gauge length of 0·625 in. without needing mechanical connections to the specimen.

Theoretical

1.   An analytical solution has been derived for the stress distribution in a long thick cylinder containing an arbitrary distribution of non-elastic strains. The non-elastic strains may include any combination of thermal, creep and plastic strains, while the boundary conditions may include any combination of internal and external pressures and any axial mean stress.

2.   The analysis has been incorporated into an Elliott 803 Autocode computer program. The program has been used, together with creep data derived from creep tests on the same batch of Nimonic alloy 105, to predict the behaviour of the tube during the process of stress redistribution arising from the initial thermal stress situation.

3.   The results of the calculation show themselves relatively insensitive to the "hardening hypothesis" used because stress changes are relatively small and because some stresses increase as others decrease[14].

4.   A simpler analysis ignoring radial and circumferential stresses (and therefore radial continuity of displacement) is shown to lead to an under-estimate of both the magnitude of the thermal stresses and the time required for them to redistribute. The simpler analysis does however give correct values for the redistributed stress pattern because in this particular case (no internal or external pressure) the radial and circumferential stresses disappear.

5.   The predicted shape of strain/time curve corresponds except at extremely small strains and times with that of a uniformly stressed specimen having the same mean stress and temperature. Thus the theory and experiment both indicate an overall creep behaviour and rupture life consistent with mean stress/mean temperature conditions.

REFERENCES

No.	Author(s)	Title, etc.
1	J. F. Barnes J. M. Clarke	The significance of creep in cooled gas turbine blades Conference on thermal loading and creep in structures and components (May 1964) Proc.I.Mech.E. p.43, Vol. 178, Part 3L
2	Henry Wiggin & Co. Ltd.	The Nimonic series of high temperature alloys
3	G. P. Tilly	Effects of varied loading paths on fatigue endurances. Part III - Some stress fatigue properties of H.46 at elevated temperatures A.R.C. Current Paper No. 788, 1964
4	S. Timoshenko	Theory of elasticity McGraw-Hill, 1934, p.366
5	A. E. Johnson J. Henderson V. Mathur	Creep under changing complex stress systems The Engineer, p.209, Vol. 206, 1958
6	A. Mendelson M. H. Hirschberg S. S. Manson	A general approach to the practical solution of creep problems Trans. A.S.M.E. Series D.J. Basic Eng. Vol. 5, No. 20, 1960
7	Y. N. Rabotnov	On the equation of state of creep Proc. Joint Int. Conference on Creep New York - London pp.2 to 117, 1963
8	A. Graham	The phenomenological method in rheology Research p.92, Vol. 6, 1953
9	A. Graham K. F. A. Walles	Relationships between long and short time properties in a commercial alloy Journal Iron and Steel Inst. p.105, Vol. 179, 1955
10	J. M. Clarke	A convenient representation of creep strain data for problems involving time-varying stresses and temperatures A.R.C. Current Paper No. 945, 1966
11	A. Phillips L. Kaechele	Combined stress tests in plasticity J.Appl.Mech. 23 (1956) 43

REFERENCES (cont'd)

No.	Author(s)	Title, etc.
12	J. Marin L. W. Hu	Biaxial plastic stress-strain relations of a mild steel for variable stress ratios Trans. A.S.M.E. 78 (1956) pp.499 to 509
13	J. C. Levy I. I. Barody	Poisson's ratio in creep using the strain-replica method Conference on thermal loading and creep in structures and components (May 1964) Proc.I.Mech.E. p.193, Vol. 178, Part 3L
14	J. M. Clarke	Conference on thermal loading and creep in structures and components Discussion at Session 4 Proc.I.Mech.E p.169, Vol. 178, Part 3L
15	J. M. Clarke	Unpublished work at N.G.T.E. 1964

TABLE I

Rupture times, reduction of area and test conditions

Note T_{25} = temperature below which 25 per cent of test duration was spent

T_{50} = temperature below which 50 per cent of test duration was spent

T_{75} = temperature below which 75 per cent of test duration was spent

T_{25}, T_{50}, T_{75} were derived from measurements by the thermocouple nearest to the rupture line

Test	Stress (t.s.i.)	T_{25} °C	T_{50} °C	T_{75} °C	Rupture time hr	% Reduction of area
A	4.0	970.0	970.2	970.7	515	18.4
B	4.0	970.6	971.6	972.7	464	18.5
C	4.0	968.5	969.4	970.0	485	18.4
D	4.0	967.1	967.3	967.5	508	17.4
E	3.96	966.5	967.5	968.3	553	17.0
F	4.0	969.0	969.4	969.8	415	16.5
G	7.0	964.7	964.9	965.0	33	29.1
H	7.0	964.5	964.6	964.8	31 < t < 32.5	(19.5)*
I	7.0	963.8	964.3	964.7	38	33.7
J	4.0	969.3	969.7	970.0	415	21.6
K	4.0	969.3	969.8	970.0	374	20.9
L	4.0	969.8	969.9	970.1	408	19.5
M	7.0	964.5	964.6	964.8	34	31.7
N	4.0	968.4	969.6	970.0	396	13.5

*This test was terminated by a power failure after 31 hr but the strain record showed that rupture would have occurred before 32.5 hr. The percentage reduction of area was for a low temperature fracture caused by the specimen's contraction while cooling.

TABLE II

Derived creep properties for Nimonic 105
fully heat treated. Cast AE 148

(For explanation of symbols see Reference 10)

Symbol	Value						Units
θ	27.8						Degrees of arc
φ	75.0						Degrees of arc
A	0.863						Natural log cycles
B	-6.430						Natural log cycles
C	0						Natural log cycles/ (ton/in^2)
at	900°C	920°C	940°C	960°C	980°C	1000°C	
D	10.45	9.81	9.29	8.81	8.39	7.97	Natural log cycles
E	-0.62	-0.680	-0.758	-0.850	-0.960	-1.10	Natural log cycles/ (ton/in^2)

APPENDIX I

Notation

a, b	arbitrary constants
c	non-elastic strain
$\mathcal{E}$	Young's modulus
e	total strain (elastic + thermal + creep)
$F(r)$, $G(r)$, $H(r)$	functions of radius
P	pressure
p, q	arbitrary constants
r	radius
R, S	constants of integration
s	mean axial stress
T	temperature
t	time
u	radial displacement
v, w	stress and temperature sensitivities of strain rate
x, y	co-ordinates of $\ln(\varepsilon/\lambda)$ versus $\ln(t/\tau)$ curve
α	temperature coefficient of linear expansion
ε	creep strain
$\bar{\varepsilon}$	effective creep strain
λ	a reference strain
υ	Poisson's ratio
σ	stress
$\bar{\sigma}$	effective stress
τ	a reference time

Notation (cont'd)

Subscripts

1, 2	before and after a time increment
1, 2, 3	axial radial and hoop directions
i, o	inside and outside surfaces
s	strain hardening hypothesis
t	time hardening hypothesis
max	maximum
mean	area mean

APPENDIX II

Calculation of stresses in a long thick-walled tube with arbitrary mean axial stress, inside and outside pressures and radial distribution of non-elastic strains

Hooke's law in the presence of non-elastic strains may be written:

$$
\left.
\begin{aligned}
e_1 &= \frac{1}{E}\sigma_1 - \frac{v}{E}(\sigma_2 + \sigma_3) + c_1 \\[2mm]
e_2 &= \frac{1}{E}\sigma_2 - \frac{v}{E}(\sigma_1 + \sigma_3) + c_2 \\[2mm]
e_3 &= \frac{1}{E}\sigma_3 - \frac{v}{E}(\sigma_2 + \sigma_1) + c_3
\end{aligned}
\right\} \qquad \dots\text{(II.1)}
$$

Elimination of σ_1 from the above and some re-arrangement gives:

$$
\sigma_2 = \frac{Ev}{(1 - 2v)(1 + v)}\Big((e_1 - c_1) + (e_2 - c_2) + (e_3 - c_3) \Big)
$$

$$
+ \frac{E}{1 + v}\Big((e_1 - c_2) \Big) \qquad \dots\text{(II.2)}
$$

$$
\sigma_2 - \sigma_3 = -\frac{E}{1 + v}\Big((e_2 - e_3) - (c_2 - c_3) \Big) \qquad \dots\text{(II.3)}
$$

The radial equilibrium condition in the absence of body forces is:

$$
\frac{d\sigma_2}{dr} + \frac{\sigma_2 - \sigma_3}{r} = 0 \qquad \dots\text{(II.4)}
$$

and the compatability condition under the assumed axisymmetric and longitudinally uniform conditions is:

$$
\left.
\begin{aligned}
e_1 &= \text{constant} \\[2mm]
e_2 &= \frac{du}{dr} \\[2mm]
e_3 &= \frac{u}{r}
\end{aligned}
\right\} \qquad \dots\text{(II.5)}
$$

Substitution from (II.5) into (II.2) and (II.3) and then from (II.2) and (II.3) into (II.4) leads to the following second order non-homogeneous ordinary differential equation for the displacement:

$$\frac{d}{dr} \left(\frac{du}{dr} + \frac{u}{r} \right) = F(r) \qquad \dots (II.6)$$

where $\quad F(r) = \frac{v}{1 - v} \frac{d}{dr} (c_1 + c_2 + c_3) + \frac{1 - 2v}{1 - v} \left(\frac{dc_2}{dr} + \frac{c_2 - c_3}{r} \right)$

$$\dots (II.7)$$

Two integrations of (II.6) lead to the form of the solution for displacement:

$$u = Rr + S \frac{r_i^2}{r} + \frac{1}{r} \int_{r_i}^{r} r \int_{r_i}^{r} F(r) \, dr \, dr \qquad \dots (II.8)$$

and for convenience the notation

$$G(r) = \int_{r_i}^{r} F(r) \, dr$$

$$H(r) = \frac{1}{r^2} \int_{r_i}^{r} r \, G(r) \, dr$$

is introduced so that (II.8) can be written

$$u = Rr + Sr_i^2 \frac{1}{r} + r H(r) \qquad \dots (II.9)$$

The problem is therefore reduced to finding the constants R, S and e_1, such that the following boundary conditions apply

(i) $\quad \sigma_{2i} = -P_i \qquad$ the inside pressure

(ii) $\quad \sigma_{2o} = -P_o \qquad$ the outside pressure $\qquad \left. \begin{array}{l} \\ \\ \\ \end{array} \right\} \quad \dots (II.10)$

(iii) $\quad 2 \int_{r_i}^{r_o} \sigma_1 r \, dr / (r_o^2 - r_i^2) = s \quad$ the mean axial stress

Substitution from (II.5) into (II.2) expresses σ_2 in terms of u and its derivative so that Equation (II.8) is then available to express σ_2 in terms of the constants R, S and e_1.

$$\sigma_2 = \frac{\mathscr{E}}{(1-2v)(1+v)}(R + ve_1) - \frac{\mathscr{E}}{(1+v)}\left(S\frac{r_i^2}{r^2} + H(r)\right)$$

$$+ \frac{\mathscr{E}(1-v)}{(1-2v)(1+v)}\left(G(r) - c_2\right) - \frac{\mathscr{E}v}{(1-2v)(1+v)}(c_1 + c_3)$$

$$\ldots(II.11)$$

Substitution for $\sigma_2 = -P_1$ at $r = r_i$ and $\sigma_2 = -P_0$ at $r = r_0$ leads to values for $(R + ve_1)$ and S

$$S = \frac{r_0^2}{r_0^2 - r_i^2}\left\{\frac{1+v}{\mathscr{E}}(P_1 - P_0) - \frac{1-v}{1-2v}G(r_0) + H(r_0)\right.$$

$$+ \frac{v}{1-2v}\left((c_{10} - c_{11}) + (c_{30} - c_{31})\right) + \frac{1-v}{1-2v}(c_{20} - c_{21})\Bigg\}$$

$$\ldots(II.12)$$

$$R + ve_1 = S(1-2v) - \frac{(1-2v)(1+v)}{\mathscr{E}}P_1 + (1-v)c_{2i} + v(c_{1i} + c_{3i})$$

$$\ldots(II.13)$$

The last two equations permit σ_2 to be found using (II.11) then σ_3 can be found from:

$$\sigma_2 - \sigma_3 = \frac{\mathscr{E}}{1+v}\left(2S\frac{r_i^2}{r^2} + 2H(r) - G(r) + (c_2 - c_3)\right) \qquad \ldots(II.14)$$

The radial and hoop stresses have now been determined but the third boundary condition has not been introduced. This can now be done by integrating the first equation in II.1.

Hence $e_1 = \dfrac{2}{r_o^2 - r_i^2} \cdot \left\{ \dfrac{1}{E} \displaystyle\int_{r_i}^{r_o} r\sigma_1 \, dr - \dfrac{v}{E} \displaystyle\int_{r_i}^{r_o} (\sigma_2 + \sigma_3) r dr + \displaystyle\int_{r_i}^{r_o} c_1 r dr \right\}$

i.e., $e_1 = \dfrac{s}{E} - \dfrac{2}{r_o^2 - r_i^2} \left\{ \dfrac{v}{E} \displaystyle\int_{r_i}^{r_o} (\sigma_2 + \sigma_3) r dr - \displaystyle\int_{r_i}^{r_o} c_1 r dr \right\}$ ....(II.15)

Sufficient information is now available to calculate σ_1 from the first equation in II.1, and the displacement function u from the solution II.8.

APPENDIX III

Some conditions required for the establishment of a steady state stress distribution in a uniaxial axisymmetric situation

The analysis which follows illustrates a number of properties of the 'fully redistributed' or 'steady state' stress pattern which is generally achieved after stress redistribution calculations.

It is shown that if the log(creep strain)/log(time) curves are of the same shape and simply displaced for different stresses and temperatures then the existence of a general steady state requires that the shape involved is a member of a family of curves containing three arbitrary constants and including as a sub-set all straight lines. A method is shown for calculating directly the redistributed solution.

It is assumed that the creep strain/time results of ordinary creep tests over a range of stresses and temperatures can be represented by a formula of the form:

$$\ln\left(\frac{\varepsilon}{\lambda}\right) = f_1\left(\ln\left(\frac{t}{\tau}\right)\right) \qquad \ldots\ldots(\text{III.1})$$

or for convenience:

$$y = f_1(x) \qquad \ldots\ldots(\text{III.2})$$

where the function f_1 does not depend on stress or temperature but λ and τ can each depend on both stress and temperature. The function f_1 is for the moment arbitrary and so are λ and τ which are the strain and time values for which y and x respectively are zero. A hyperbolic relation between x and y is used in Reference 10 and also in the theoretical work described in this Report.

It can be shown that the corresponding expression for strain rate is:

$$\frac{d\varepsilon}{dt} = \frac{dy}{dx} \cdot \exp(y - x) \cdot \frac{\lambda}{\tau} \qquad \ldots\ldots(\text{III.3})$$

or

$$\frac{d\varepsilon}{dt} = f_2(x) \cdot \frac{\lambda}{\tau} \qquad \ldots\ldots(\text{III.4})$$

where

$$f_2(x) = \frac{dy}{dx} \cdot \exp(y - x) \qquad \ldots\ldots(\text{III.5})$$

Now in a uniaxial axisymmetric stress situation in which neither the stress nor temperature are changing with time the creep strain rate (say $\dot{\varepsilon}_1$) must be the same at all positions, so that

$$f_2(x) = \dot{\varepsilon}_1 \tau/\lambda \qquad \qquad \dots\dots(III.6)$$

where in general τ/λ and x will be different at different positions.

Some time later although τ/λ remains constant (because stresses and temperatures are constant) the strain rates (say $\dot{\varepsilon}_2$) common to all positions might be different, so that

$$f_2(x + \Delta x) = \dot{\varepsilon}_2 \tau/\lambda \qquad \qquad \dots\dots(III.7)$$

Now
$$\Delta x = \ln\left(1 + \frac{\Delta t}{t}\right) \qquad \qquad \dots\dots(III.8)$$

which is independent of x and is the same at all points hence

$$\frac{f_2(x + \Delta x)}{f_2(x)} = \frac{\dot{\varepsilon}_2}{\dot{\varepsilon}_1} \text{ for all } x, \qquad \qquad \dots\dots(III.9)$$

i.e., the proportional change in f_2 with x does not depend on the instantaneous value of f_2. The most general function with this property is the exponential function which may be written:

$$f_2(x) = \exp(ax + b) \text{ where } a, b \text{ are constants}$$

$$\dots\dots(III.10)$$

or equivalently, and more conveniently in this case:

$$f_2(x) = p \exp\left((p - 1) x + q\right) \qquad \qquad \dots\dots(III.11)$$

where p, q are constants. Comparison with (III.5) yields the differential equation

$$\exp(y) \cdot \frac{dy}{dx} = p \exp(px + q) \qquad \ldots\text{(III.12)}$$

Integration of this equation gives:

$$y = \ln\left(\exp(px + q) + \exp(y_{-\infty}) \right) \qquad \ldots\text{(III.13)}$$

where $y_{-\infty}$ is the value of y when $x = -\infty$.

An important special case of (III.13) is the straight line

$$y = px + q \qquad \ldots\text{(III.14)}$$

which corresponds to a strain/time relation of the form

$$\varepsilon \propto t^p \qquad \ldots\text{(III.15)}$$

and assumes zero creep strain at zero time.

Substitution from (III.11) into (III.4) gives

$$\frac{d\varepsilon}{dt} = p \exp\left((p - 1) x + q \right) \cdot \frac{\lambda}{\tau} \qquad \ldots\text{(III.16)}$$

i.e.,

$$\frac{d\varepsilon}{dt} = p \exp(q) \cdot t^{p-1} \cdot \frac{\lambda}{\tau^p} \qquad \ldots\text{(III.17)}$$

In the general case when both λ and τ vary with stress and temperature the steady state stress pattern must therefore satisfy (because the other term in (III.17) is the same for all elements):

$$\frac{\lambda}{\tau^p} = \text{constant} \qquad \ldots\text{(III.18)}$$

and the constant can be obtained from the requirement that the integrated stress be equal to the applied load. The solution therefore depends on p unless λ is constant.

Simple example

Assuming the following variations of λ and τ with stress and temperature:

$$\left.\begin{array}{rl} \lambda &= \text{constant} \\ \tau &= \tau' \exp\left(v(\sigma - \sigma') + w(T - T')\right) \end{array}\right\} \qquad \ldots(III.19)$$

Here τ', σ', T' are typical constant values for the time scale, stress and temperature of the problem while v and w represent sensitivities of τ to departures from σ' and T'.

Then for constant λ/τ^p as required by (III.18) for a steady state solution

$$\tau = \text{constant} \qquad \ldots(III.20)$$

and from (III.19)

$$v(\sigma - \sigma') + w(T - T') = \text{constant} = K \qquad \ldots(III.21)$$

Integrating with respect to area gives:

$$v \int \sigma dA + w \int T dA = (K + v\sigma' + wT') \cdot \int dA \qquad \ldots(III.22)$$

i.e.,

$$v(\sigma_m - \sigma') + w(T_m - T') = K \qquad \ldots(III.23)$$

where σ_m and T_m are area mean values of stress and temperature.

From (III.23) and (III.19) it follows that the effective time scale factor τ for the non-uniform system corresponds to that obtainable from a uniform stress situation at the same mean stress and temperature.

It should be emphasised that the relatively simple expressions (III.19) which led to this conclusion only apply for rather limited departures of stress and temperature from the σ', T' values. Nevertheless the analysis serves to illustrate that the strain accumulation after redistribution corresponds roughly with mean stress/mean temperature conditions and the solution of (III.18) with more accurate forms of (III.19) gives a useful technique for the direct calculation of steady state stress patterns from applied temperature patterns.

RIGID ENDS

CONSTANT
TENSILE
LOAD

700°C

600°C

700°C

TENSILE
STRESS

600°C BAR

700°C BARS

0

TIME

INITAL STRESS DIFFERENCE
CAUSED BY DIFFERENT
THERMAL EXPANSIONS

FINAL STRESS DIFFERENCE
CAUSED BY DIFFERENT
RESISTANCES TO CREEP
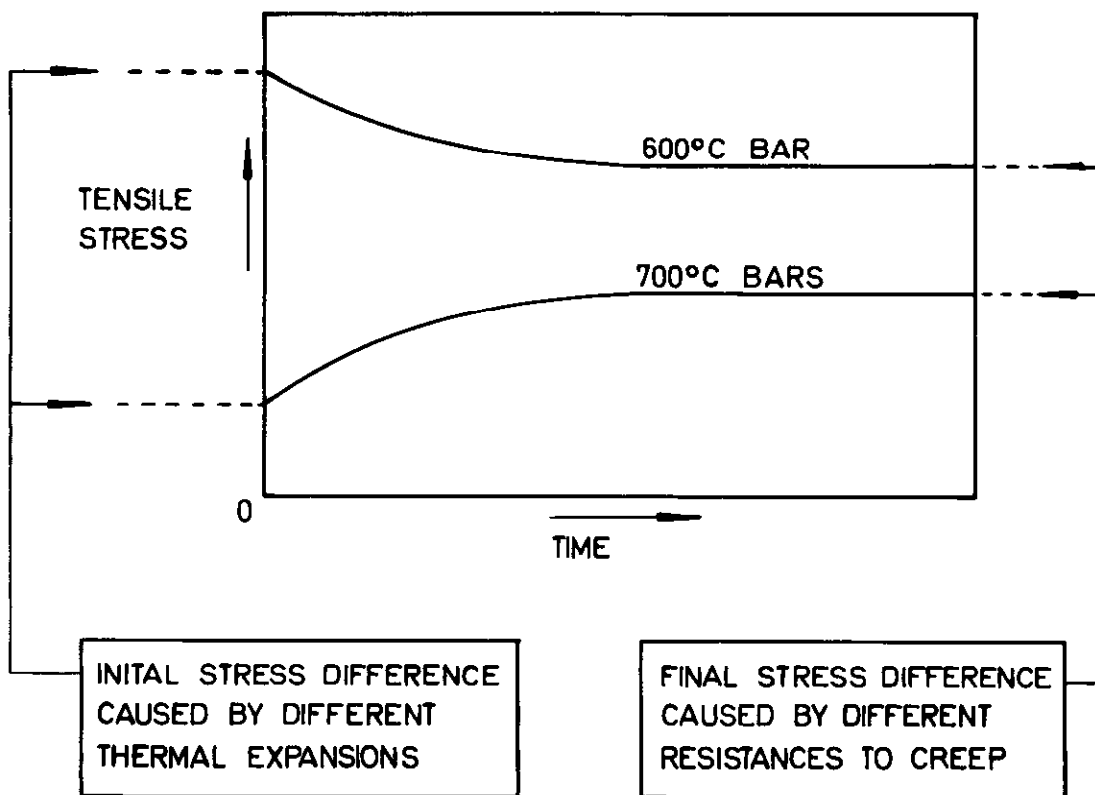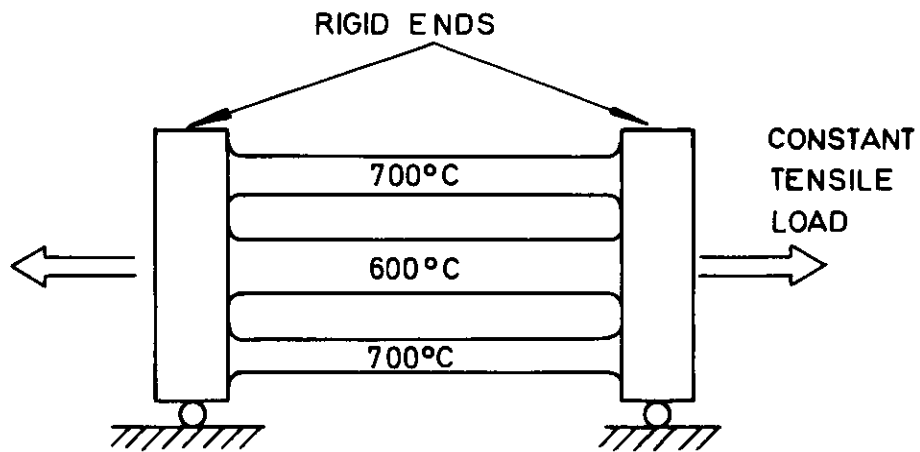
FIG 1 STRESS REDISTRIBUTION IN A SIMPLE TENSILE SYSTEM

TENSIONING WHEEL

SUPPORT
FRAME

INSULATING
COUPLING

CONTROLLED
A C SUPPLY

FLEXIBLE
CONECTORS

HEATED
TUBULAR
SPECIMEN

INSULATING
COUPLING

TRANSFORMER

LOADING BEAM
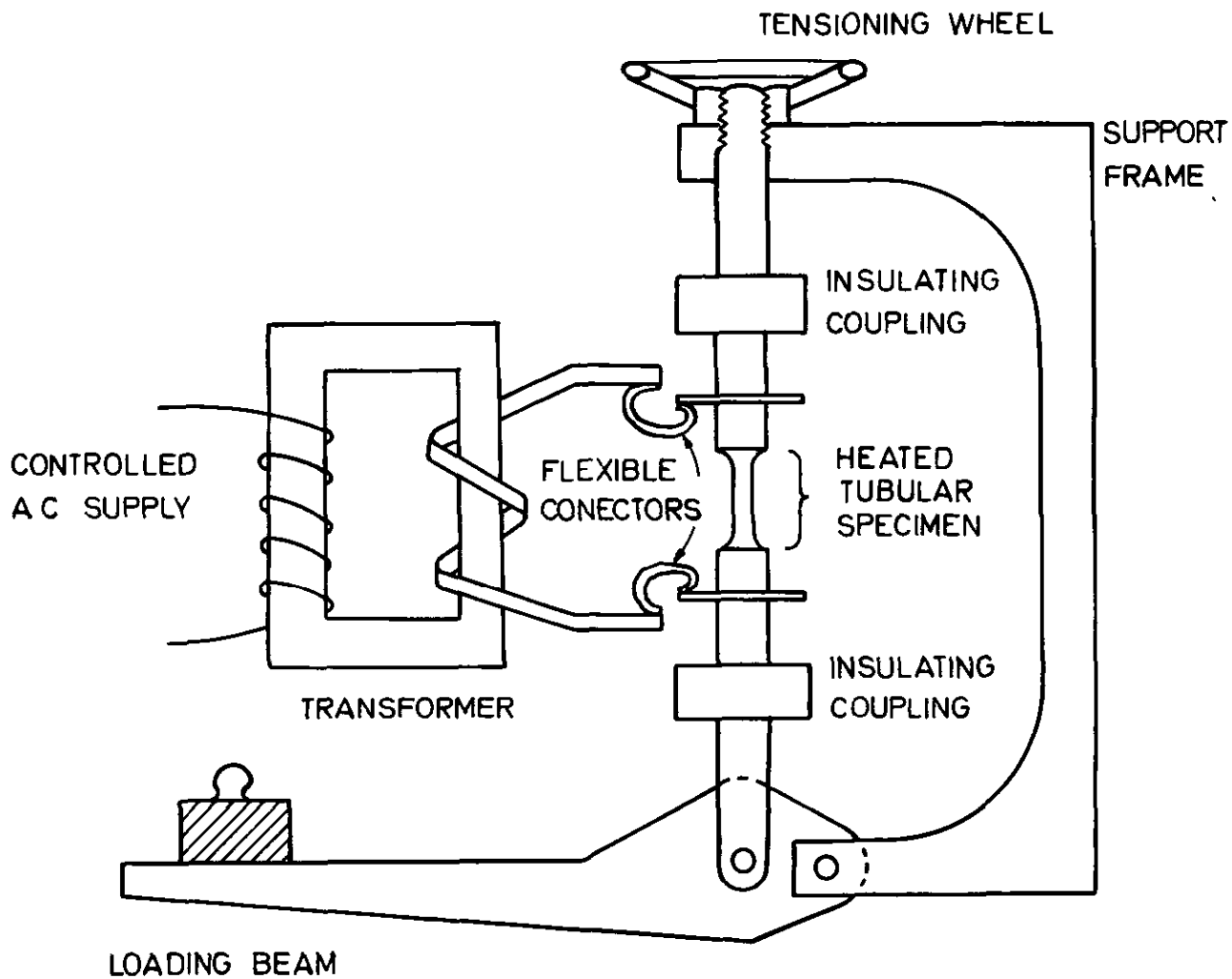
FIG 2 SCHEMATIC ARRANGEMENT OF APPARATUS
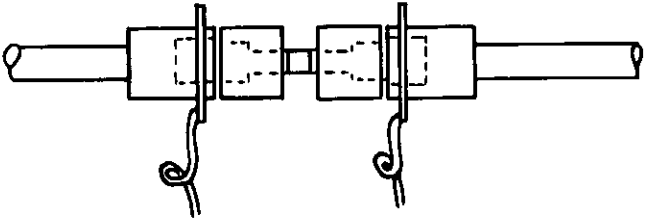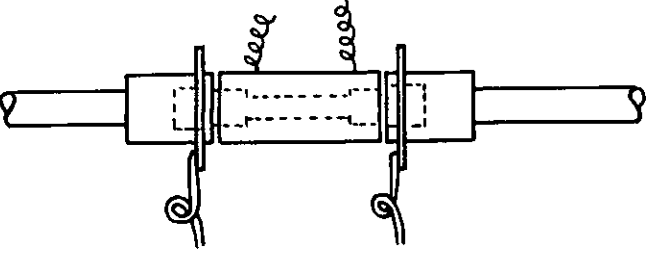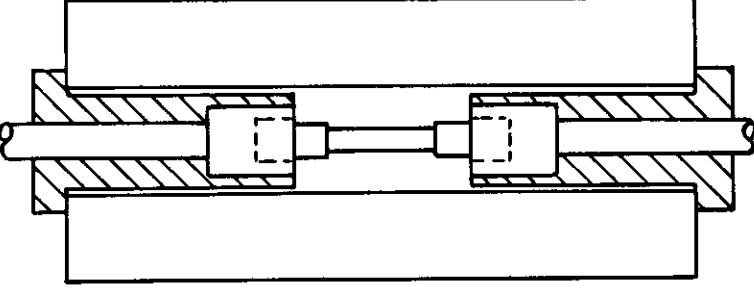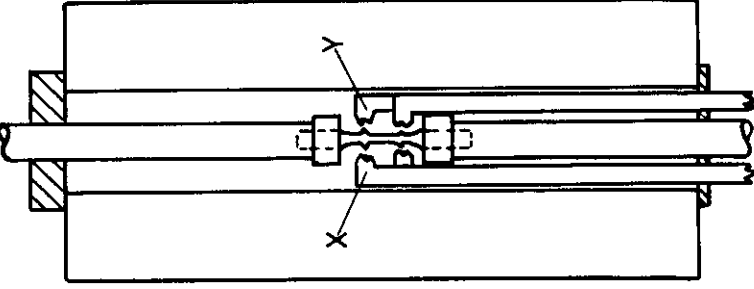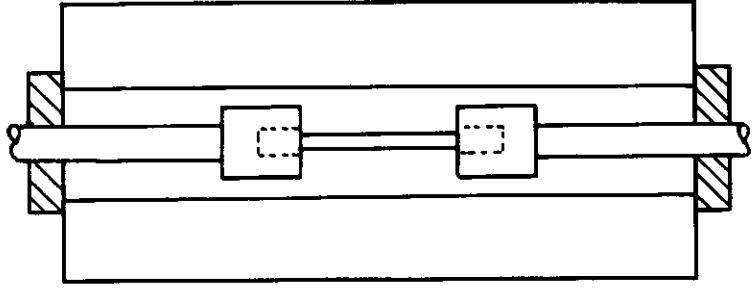
TYPE 1	TYPE 2	TYPE 3	TYPE 4	TYPE 5
TUBE SPECIMEN DIRECT ELECTRIC HEATING CENTRE PORTION FREE TO RADIATE RADIAL TEMP GRADIENT INSIDE TEMP 970°C	TUBE SPECIMEN DIRECT ELECTRIC HEATING CENTRE PORTION ALSO HEATED BY AUXILIARY ELEMENT NO RADIAL TEMP GRADIENT SAME MEAN TEMP AS TYPE 1	TUBE SPECIMEN FURNACE HEATED NO RADIAL TEMP GRADIENT. TEMP 970°C	SOLID CYLINDRICAL SPECIMEN FURNACE HEATED SOME TESTED AT 970°C 4 TON/IN^2 OTHERS AT 965°C 7 TON/IN^2 EXTENSOMETERS (X,Y) ATTACHED	SOLID CYLINDRICAL SPECIMEN. FURNACE HEATED SOME TESTED AT 970°C 4 TON/IN^2 OTHERS AT 965°C 7 TON/IN^2
TESTS A,B,C,	TESTS D,E,	TEST F,	TESTS G,H,I,J,K,L,	TESTS M,N,

FIG 3 EXPERIMENTAL ARRANGEMENTS

MINIATURE RESISTANCE
THERMOMETER

THERMOCOUPLES
LIGHTLY WELDED TO
INSIDE OF TUBE

TWO CIRCUMFERENTIAL
PLATINUM WIRES (010 DIA)
LIGHTLY SPOT WELDED TO
OUTSIDE OF TUBE MARKING
EXTENT OF GAUGE LENGTH

1
2
3

ASBESTOS WRAPPED
COLLAR TO REDUCE
END HEAT LOSSES
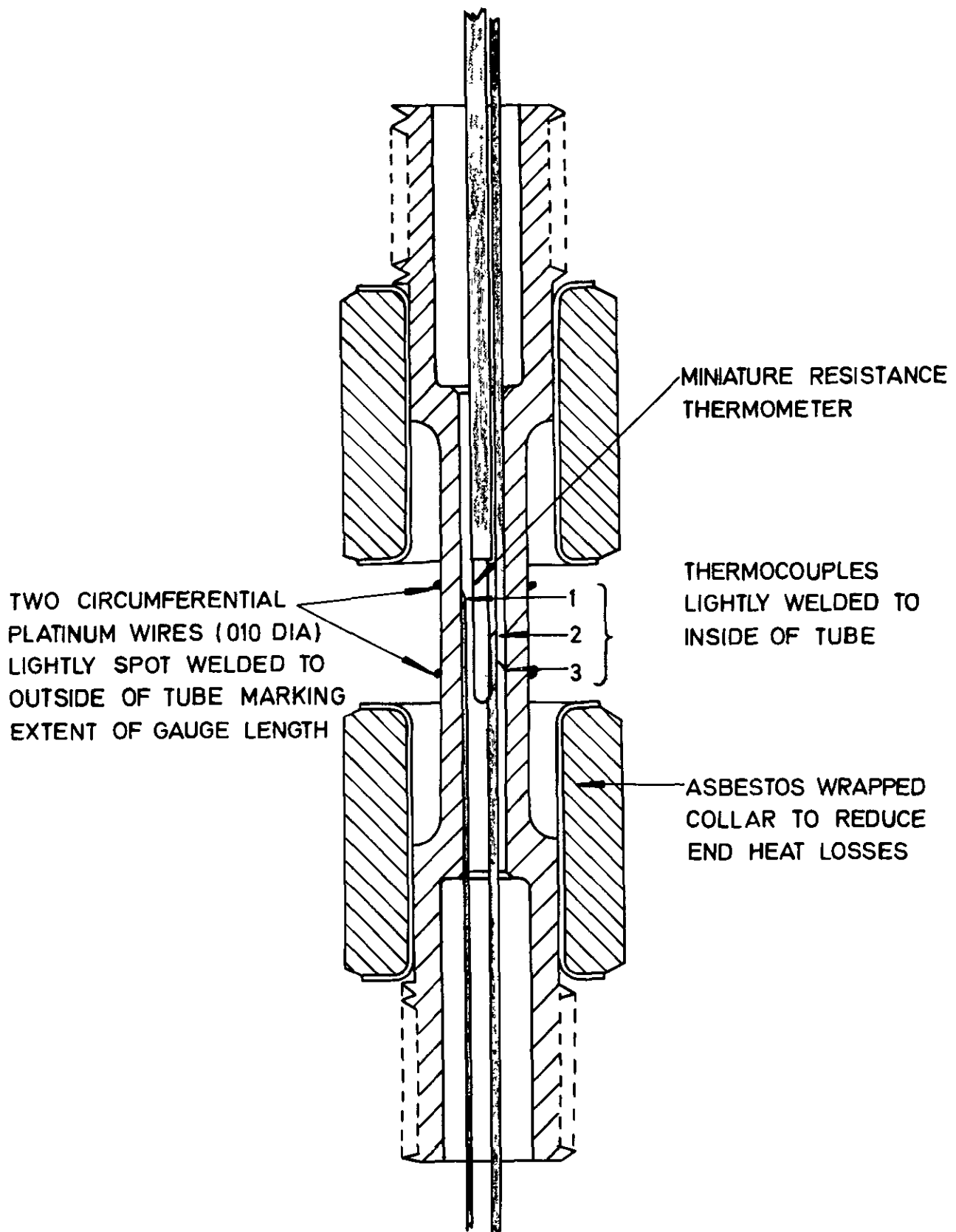
FIG 4 ARRANGEMENT NO 1 SHOWING INSTRUMENTATION
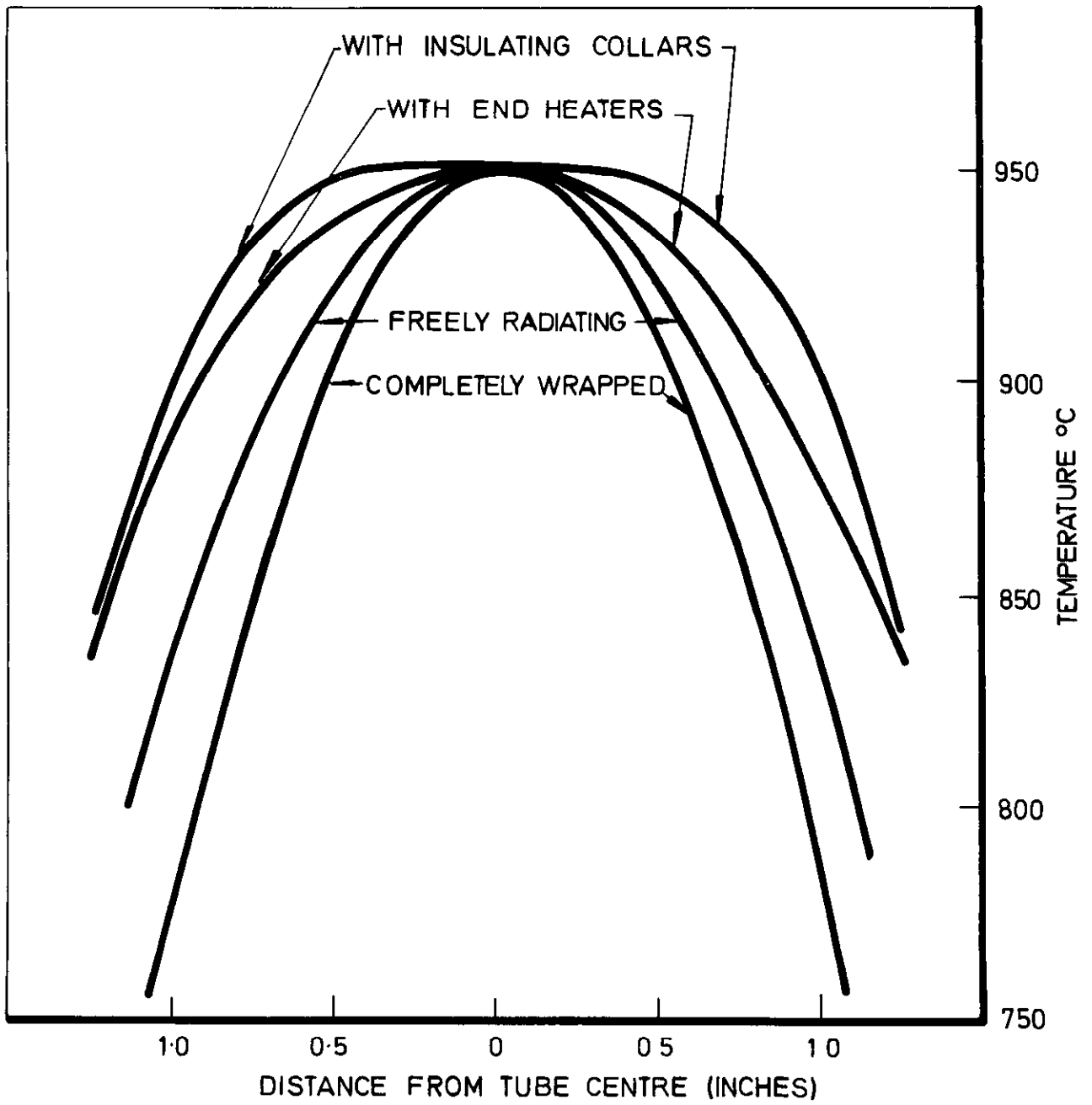
FIG 5 LONGITUDINAL TEMPERATURE PROFILES

FIG 6 OPTICAL EXTENSOMETER

FILTER

ROTATABLE GLASS BLOCK

INCLINED GLASS BLOCKS
(FIXED TO SUIT GAUGE LENGTH)

TELESCOPE

EYE

GAUGE
LENGTH

PIVOT

MICROMETER FOR STRAIN MEASUREMENT

~ 12"
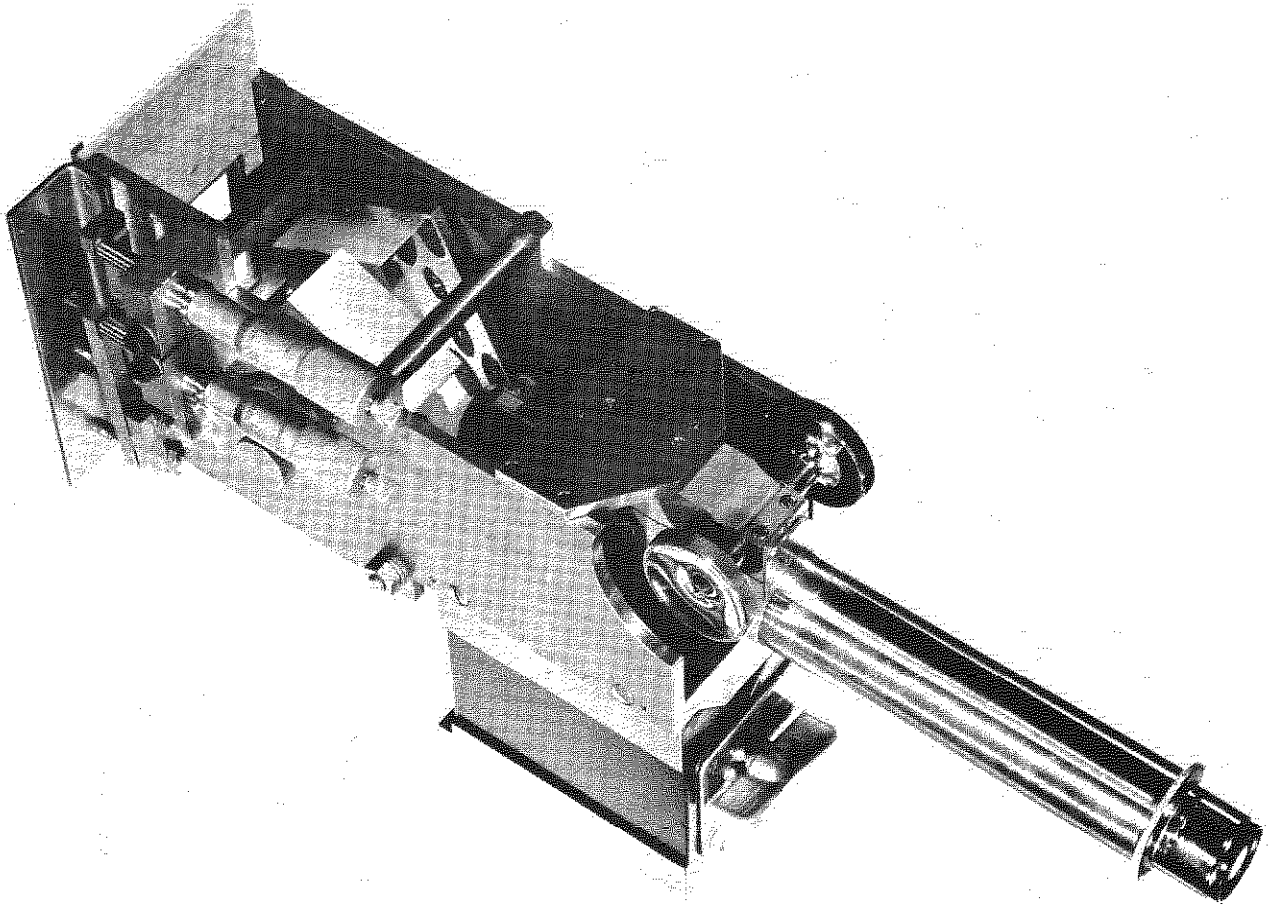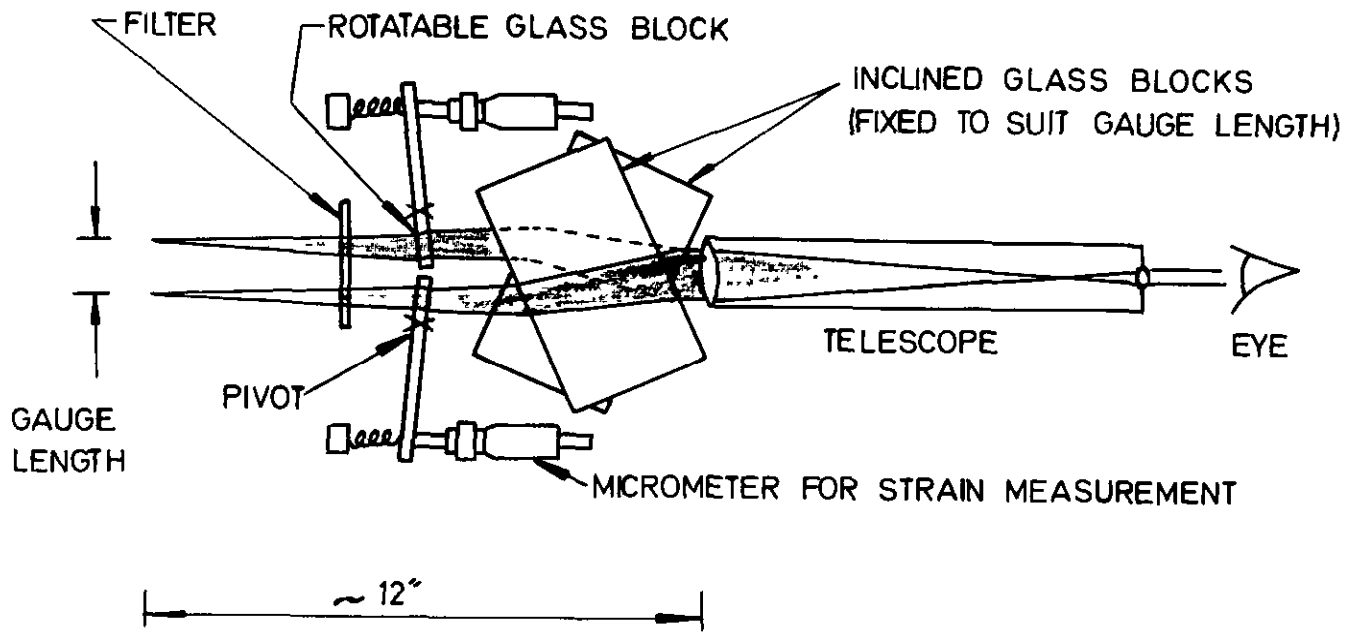
FIG 7 SCHEMATIC ARRANGEMENT SHOWING PRINCIPLE
OF OPTICAL EXTENSOMETER

T_{25} ι e 0 25 OF TEST TIME BELOW THIS TEMP

T_{50} " 0 50 " " " " " "

T_{75} " 0 75 " " " " " "

FOR LETTER CODE SEE FIGURE 21

A
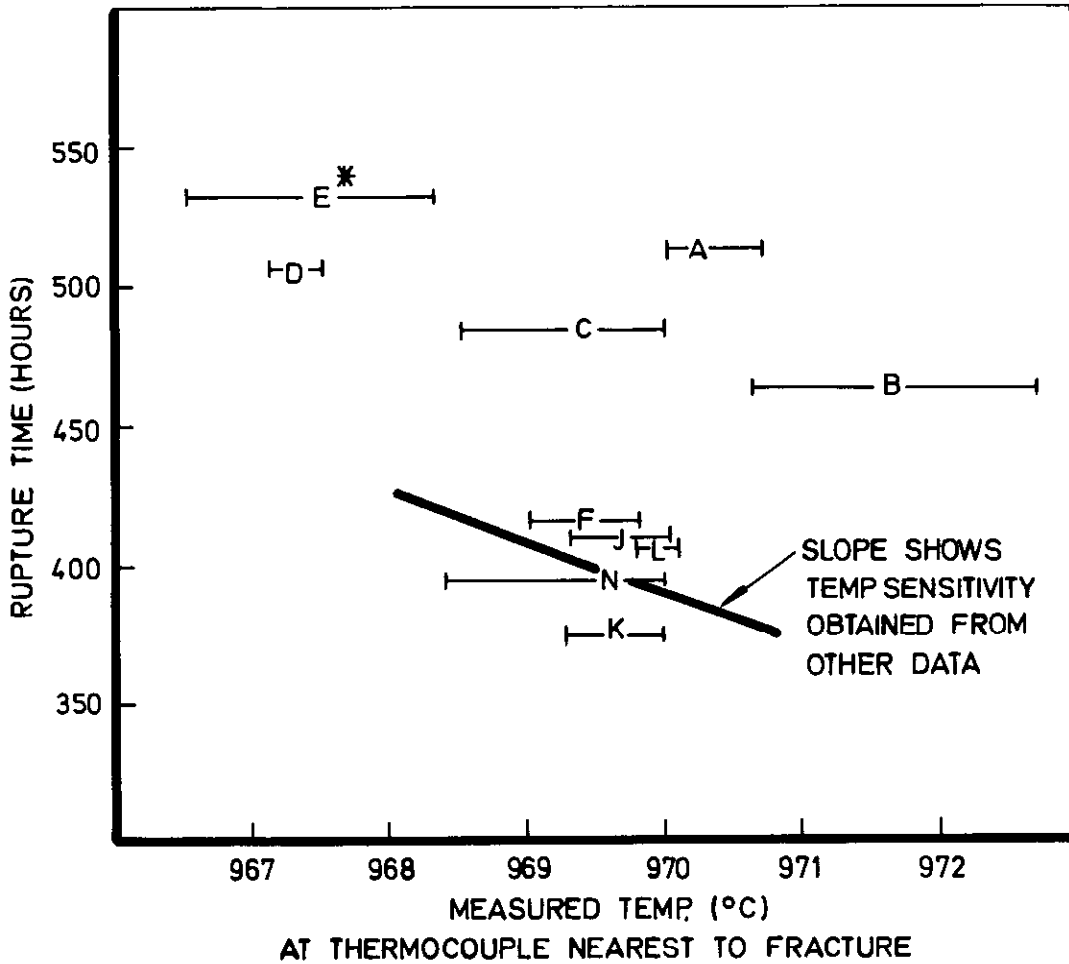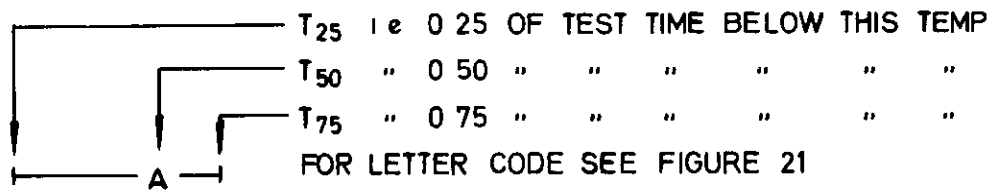
* RUPTURE TIME CORRECTED TO 4 TON/IN^2 FROM 3·96 TON/IN^2

FIG 8 RUPTURE TIMES FOR SPECIMENS STRESSED TO 4TON/IN^2

SLOPE SHOWS
TEMP SENSITIVITY
OBTAINED FROM
OTHER DATA
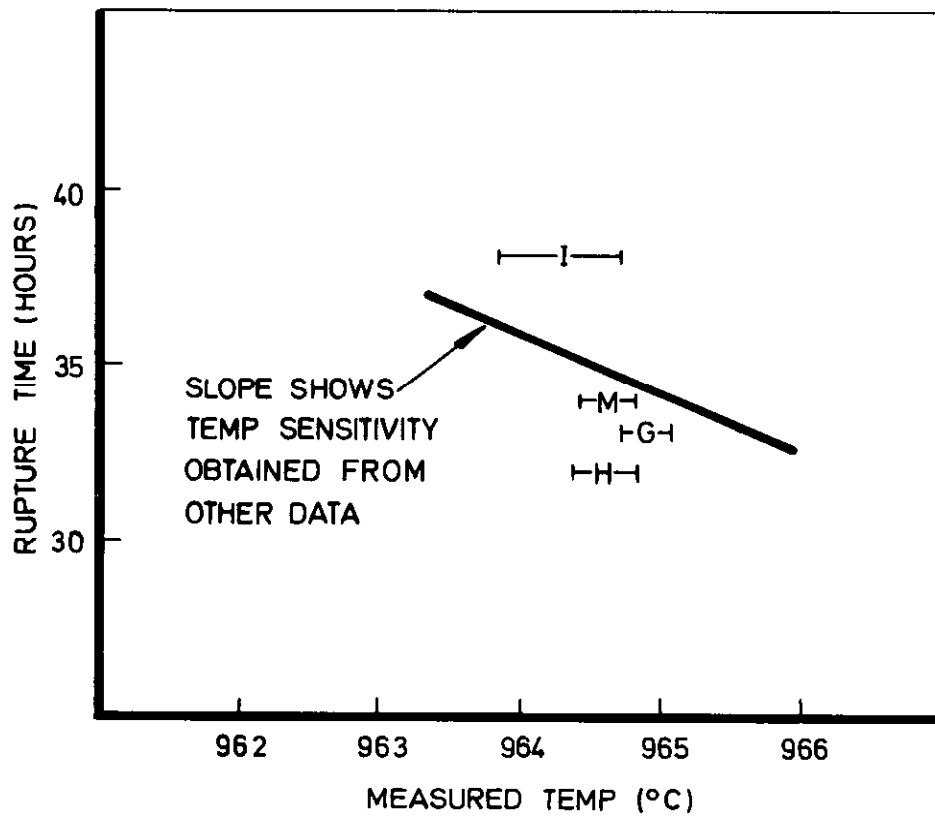
FIG 9 RUPTURE TIMES FOR SPECIMENS STRESSED TO 7 TON/IN^2
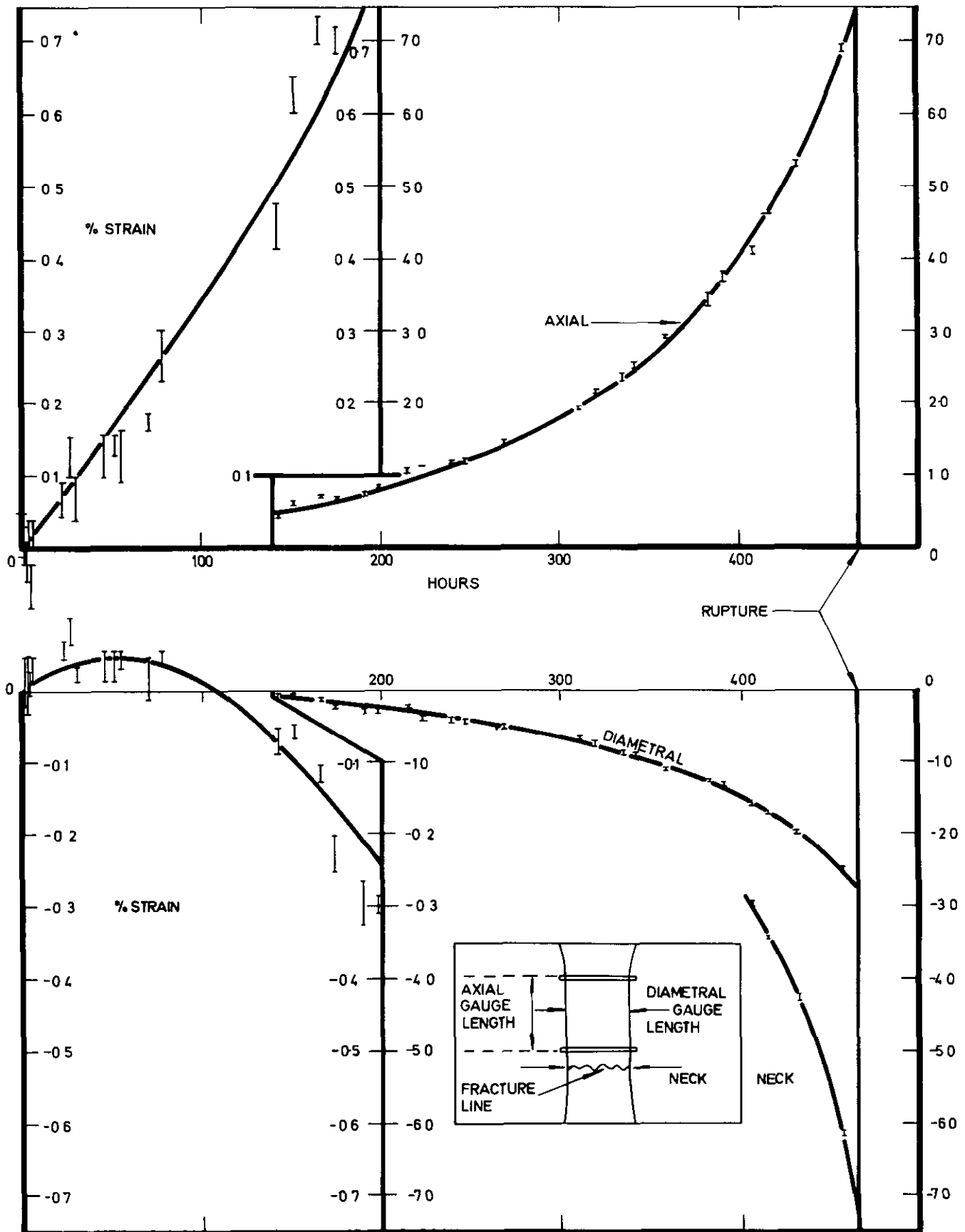
FIG 10 OPTICAL EXTENSOMETER STRAIN RESULTS — SPECIMEN B
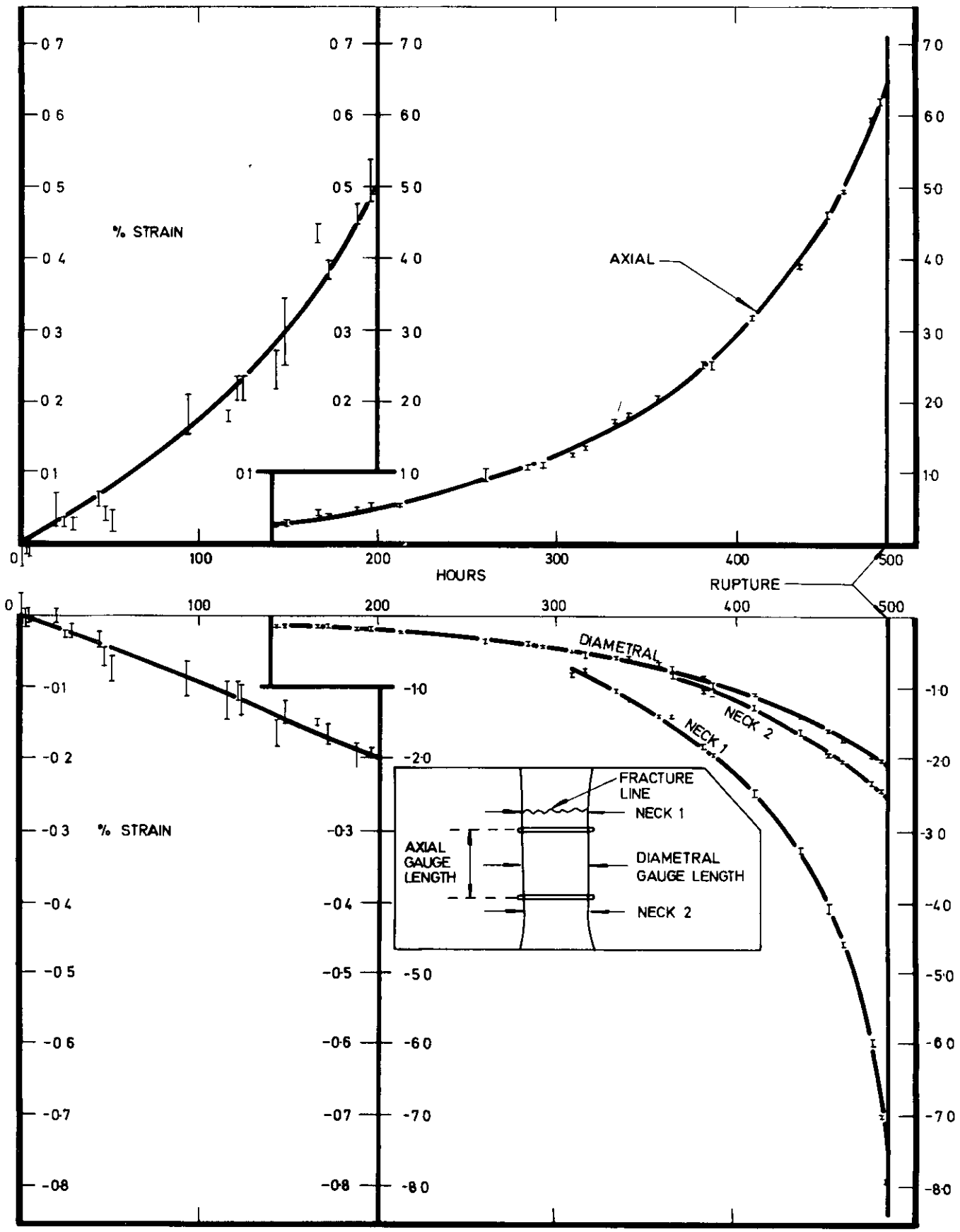
FIG 11 OPTICAL EXTENSOMETER STRAIN RESULTS- SPECIMEN C
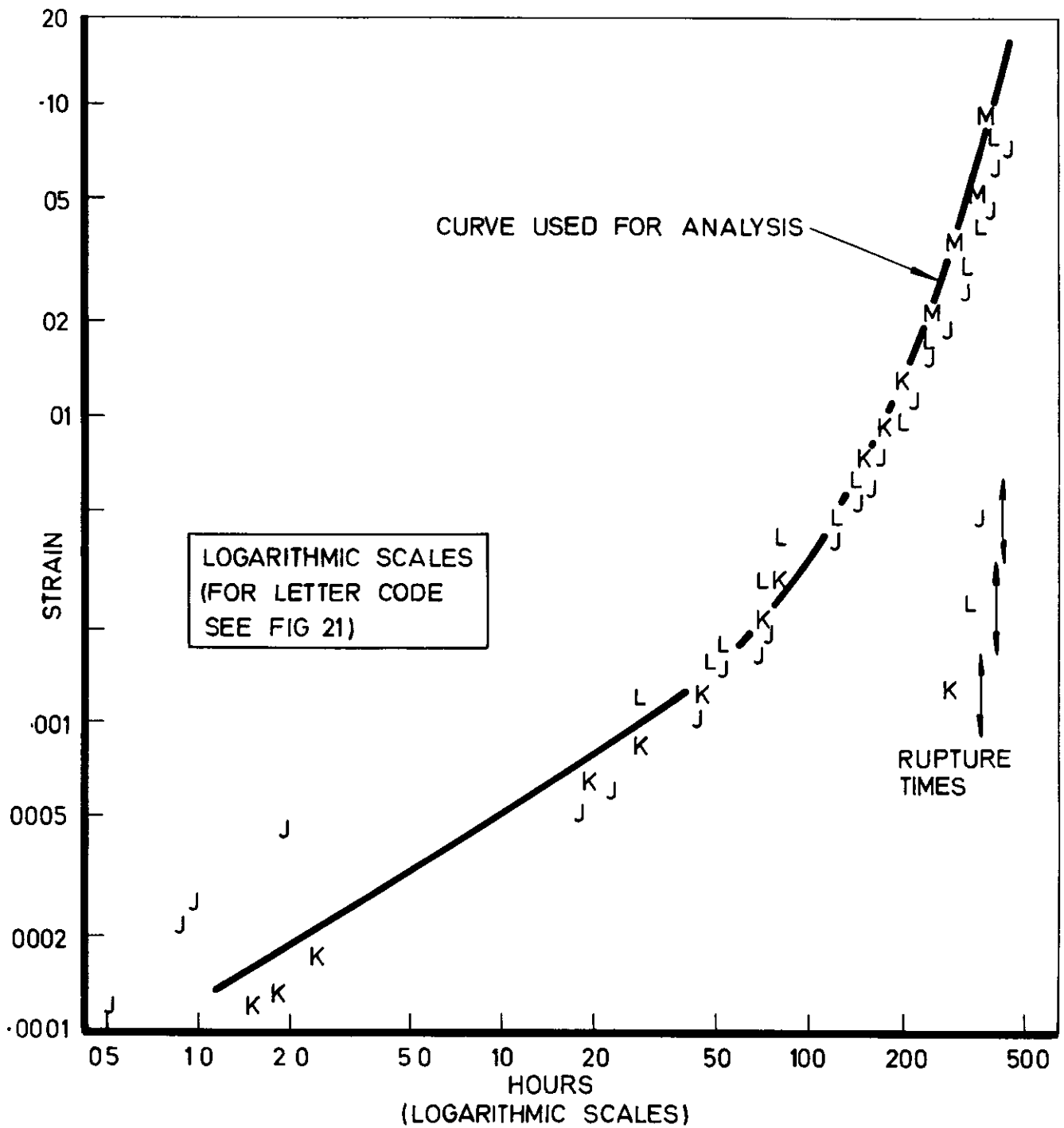
FIG 12 STRAIN RECORDS FOR TESTS AT 970°C, 4 TON/IN^2
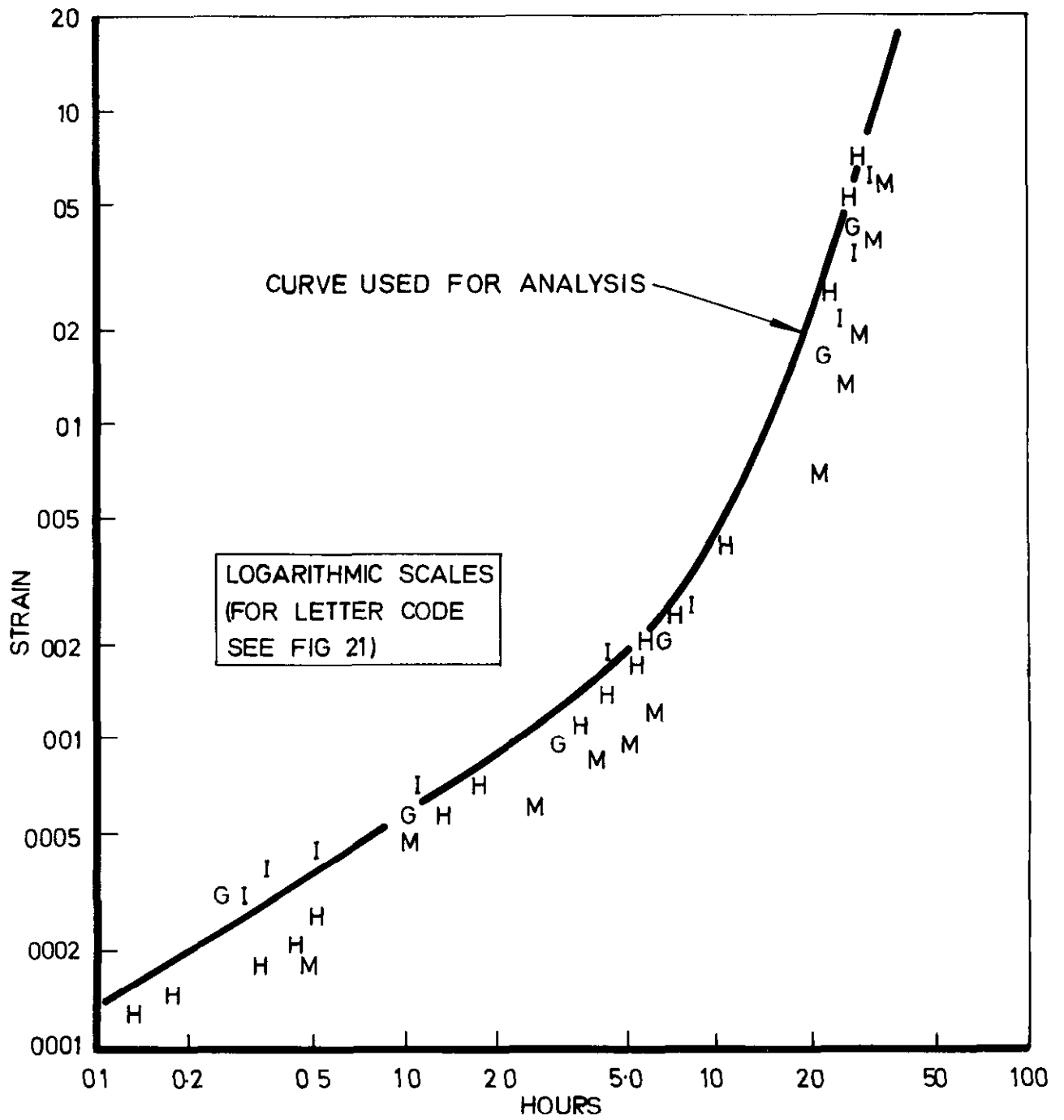
FIG 13 STRAIN RECORDS FOR TESTS AT 965°C, 7-TON/IN^2

RADIUS ————►   OUTER SURFACE
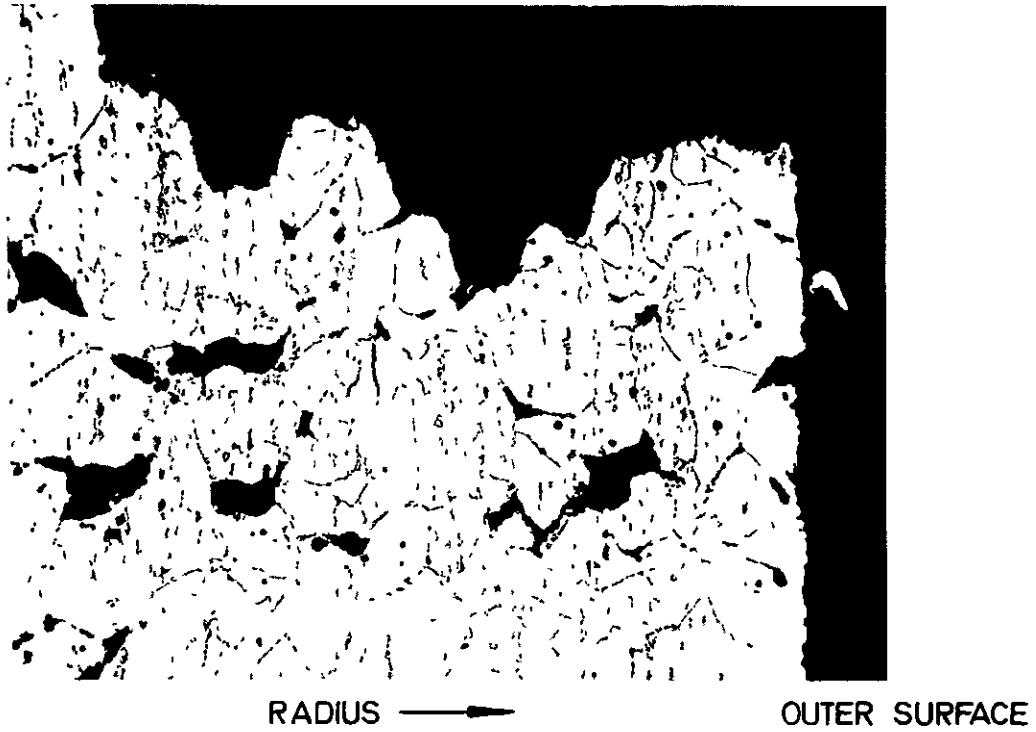
FIG 14 RADIAL SECTION THROUGH SPECIMEN C
SHOWING FRACTURE SURFACE (X 100)
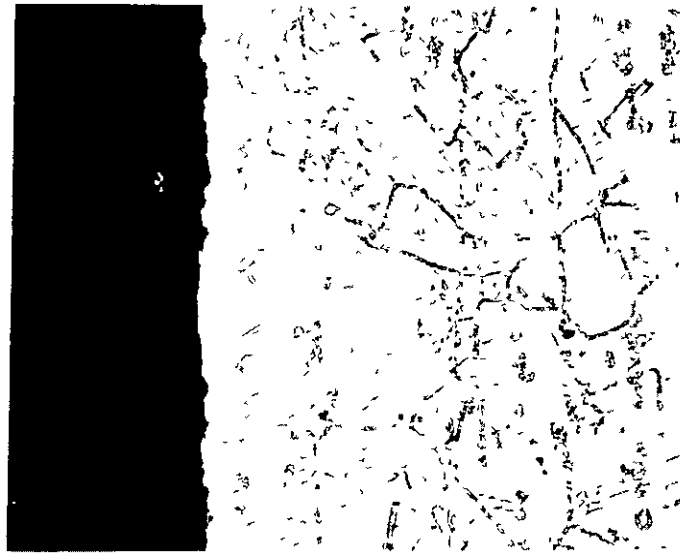
SURFACE   ──────RADIUS

INSIDE SURFACE (X 200)
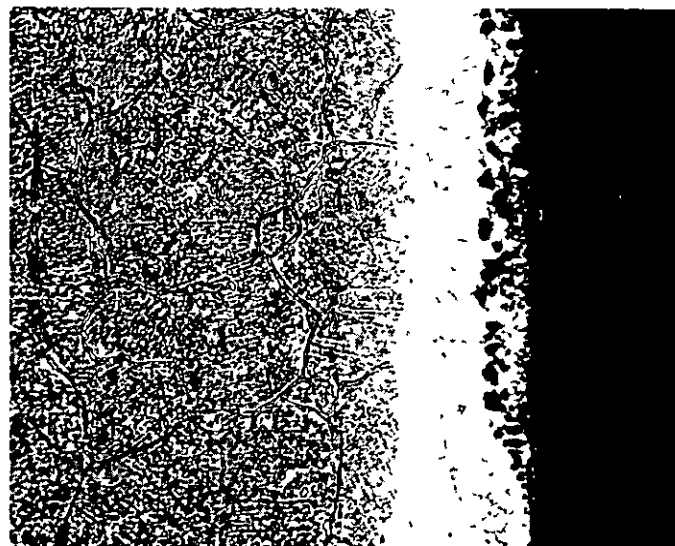
RADIUS ──────   SURFACE

OUTSIDE SURFACE (X 200)

FIG 15 RADIAL SECTIONS THROUGH SPECIMEN C SHOWING
OXIDATION AT INSIDE AND OUTSIDE SURFACES (X 200)

TUBE CROSS SECTION

RADIAL AXIAL HOOP

TEMPERATURE (°C)

970

965

960

TEMPERATURE

TENSILE STRESS (TSI)

5

4

3

2

1

0

-1

AXIAL

MORE THAN 100 HOURS

10 HOURS

INITIAL

MEAN AXIAL
STRESS

INITIAL

10 HOURS

MORE THAN 100 HOURS
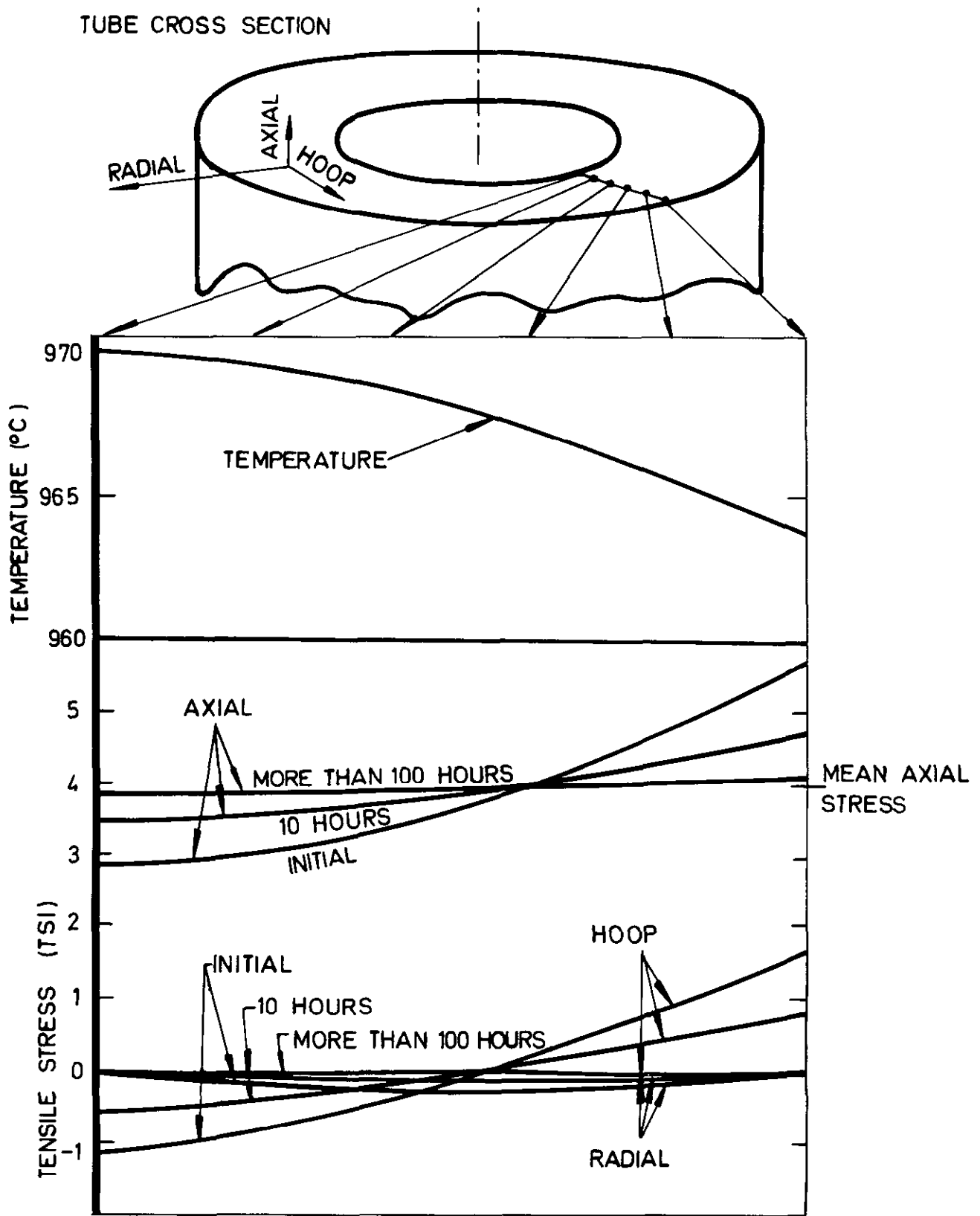
HOOP

RADIAL

FIG 16 CALCULATED TEMPERATURE AND STRESS PROFILES
BEFORE DURING AND AFTER REDISTRIBUTION
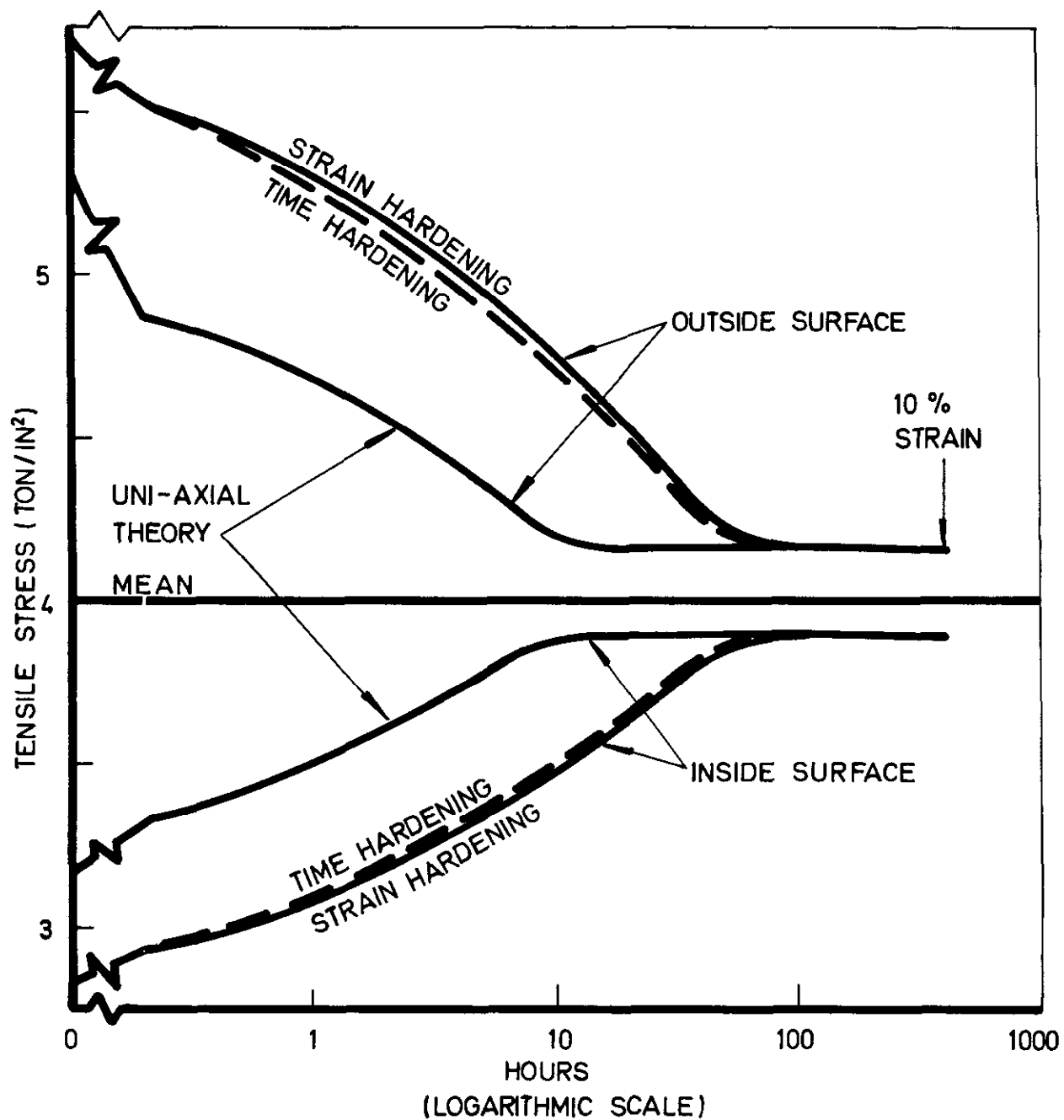
FIG 17 REDISTRIBUTION OF AXIAL STRESSES
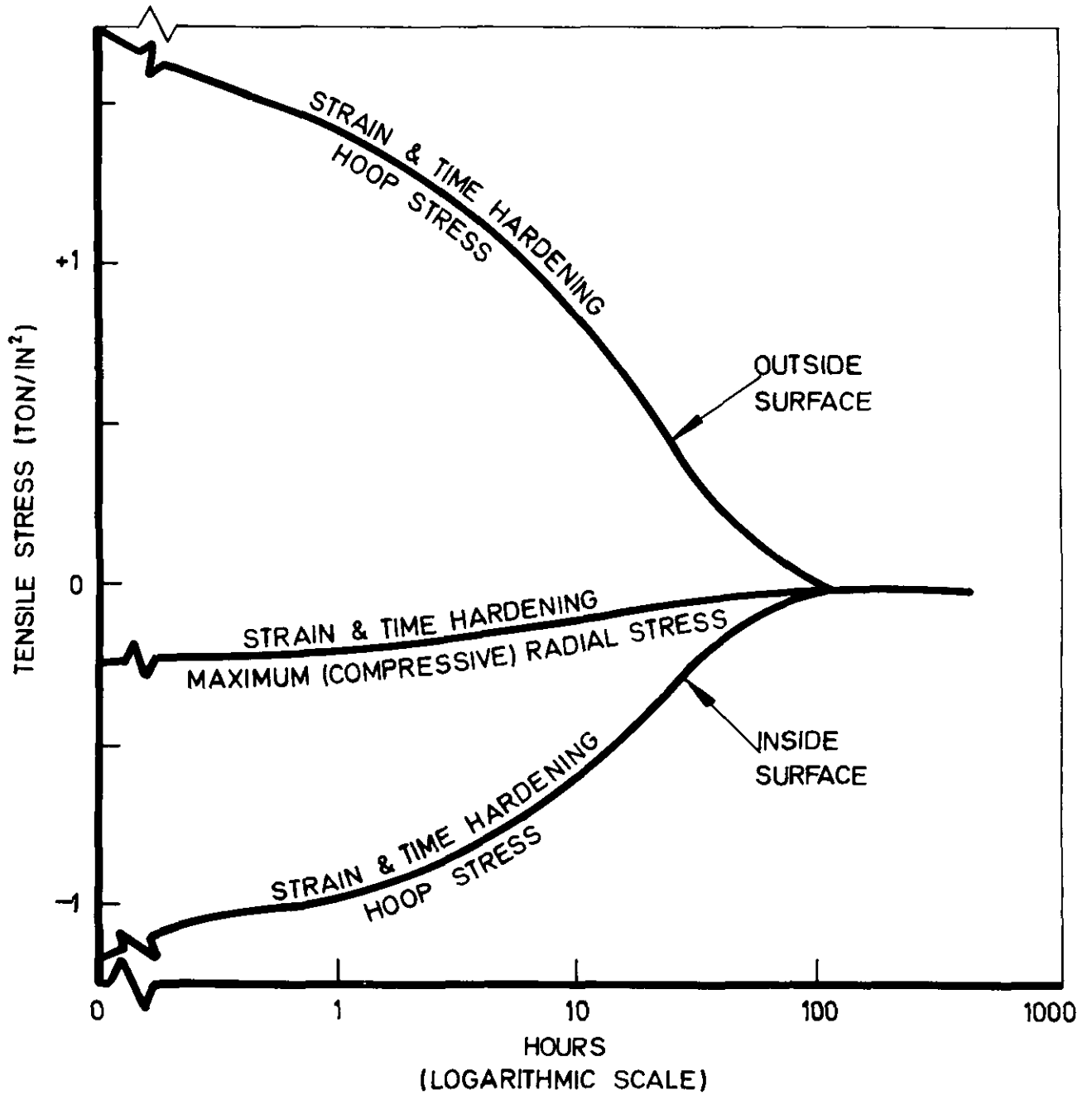
FIG 18 REDISTRIBUTION OF HOOP AND RADIAL STRESSES
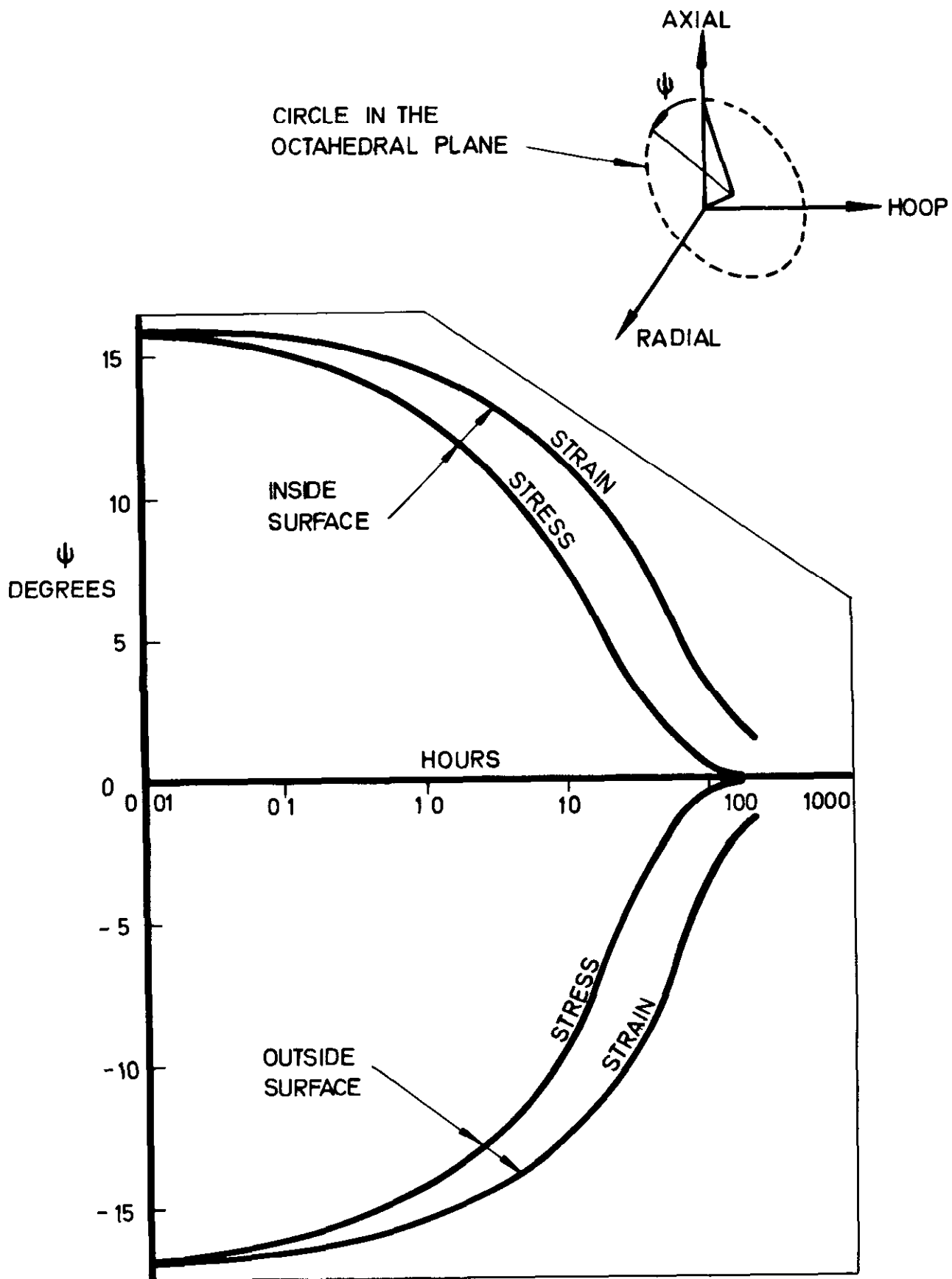
FIG 19 DIRECTIONS IN OCTAHEDRAL PLANE OF STRESSES
AND CREEP STRAINS

ARRANGEMENT TYPE	CODE	MEAN STRESS	RADIAL MEAN TEMPERATURE	STRAIN MEASURED	RUPTURE TIME
1	A	4 TON/IN²	967·4 °C	NO	515 HR
1	B	4	967 4	YES	464
1	C	4	967·4	YES	485
2	D	4	967 4	NO	508
2	E	3 96	967 4	NO	515
3	F	4	970	NO	415
4	G	7	965	YES	33
4	H	7	965	YES	32
4	I	7	965	YES	38
4	J	4	970	YES	415
4	K	4	970	YES	374
4	L	4	970	YES	408
5	M	7	965	YES	34
5	N	4	970	NO	396

FIG 21 KEY TO RESULTS
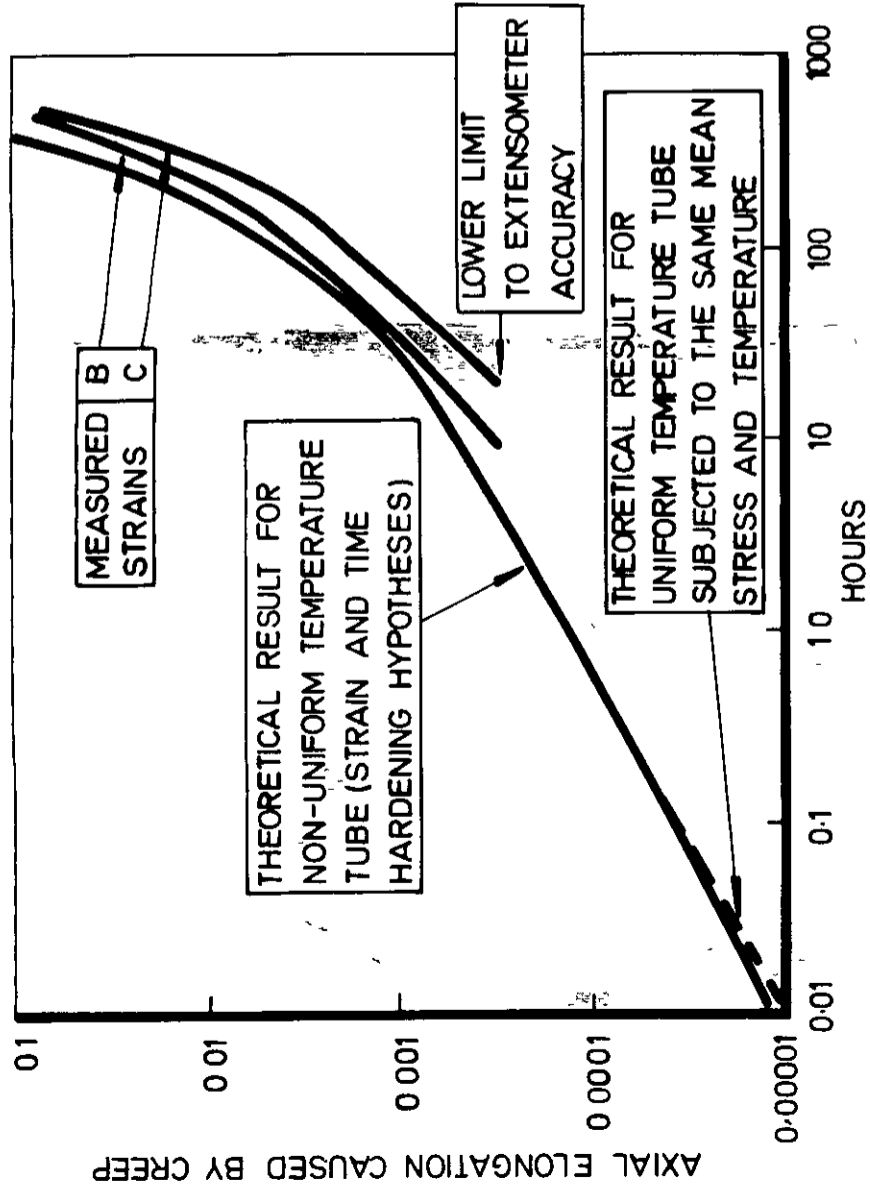
FIG 20 COMPARISON OF MEASURED AND CALCULATED ELONGATIONS

A.R.C. C.P. No. 1024   539.434:539.319
June, 1967
Clarke, J. M.

AN INVESTIGATION OF STRESS REDISTRIBUTION CAUSED BY CREEP
IN A THICK-WALLED CIRCULAR CYLINDER SUBJECTED
TO AXIAL AND THERMAL LOADING

        A thick-walled tube was subjected to an axial load and a radial
temperature distribution which caused thermal stresses. The creep strains
and the eventual rupture times were observed and compared with conventional
creep tests and theoretical analysis. Theory suggested and experiments
confirmed that stress redistribution caused the overall strain behaviour to
approach that for the mean axial stress and the mean radial temperature.

        Description of the experimental technique and apparatus includes a
novel and simple optical extensometer. Appendices contain a complete
analytic treatment of the triaxial stress problem in a long thick tube in

                                                                    P.T.O.

---

the presence of an arbitrary distribution of non-elastic strains,
and a treatment of some conditions under which stress-redistribution
calculations can lead to a "steady state" or "fully redistributed"
stress pattern.

A less rigorous theoretical treatment which ignores radial
constraints is shown to lead to an under-estimate of the thermal
stresses and of the time required for stress redistribution to
occur.